Subsurface geological and geophysical data from the Po Plain and the northern Adriatic Sea (north Italy)

Michele Livani [1], Lorenzo Petracchini[1], Christoforos Benetatos[2], Francesco Marzano[2], Andrea Billi[1], Eugenio Carminati[3], Carlo Doglioni[3,4], Patrizio Petricca[5], Roberta Maffucci[3,4], Giulia Codegone[2], Vera Rocca[2], Francesca Verga[2], Ilaria Antoncecchi[6]

[1]Consiglio Nazionale delle Ricerche, IGAG, Roma, Italy
[2]Politecnico di Torino, Dipartimento di Ingegneria dell'Ambiente, del Territorio e delle Infrastrutture, Torino, Italy
[3]Sapienza Università di Roma, Dipartimento di Scienze della Terra, Roma, Italy
[4]Istituto Nazionale di Geofisica e Vulcanologia, Osservatorio Nazionale Terremoti, Roma, Italy
[5]ISPRA Servizio Geologico d'Italia, Via Vitaliano Brancati, 48, 00144 Roma, Italy
[6]Ministero della Transizione Ecologica, Direzione Generale per le Infrastrutture e la Sicurezza, Roma, Italy

Correspondence to: Lorenzo Petracchini (lorenzo.petracchini@igag.cnr.it)

Abstract. The Po Plain (Italy) is one of the most densely populated and productive regions of Europe, characterized by a flourishing economy (also linked to strategic subsurface resources) and several world cultural and natural heritage sites. The coupling of social-economic interests with geological hazards (i.e., seismic, subsidence and flooding hazards) in this area requires accurate knowledge of the subsurface geology, active geological processes, and impact of human activities on natural environments to mitigate the potential natural and anthropic risks.

Most data unveiling the subsurface geology of this region were produced by the hydrocarbon exploration industry. Po Plain hosts indeed many hydrocarbon fields that were discovered since the early 1950s giving rise to the subsurface exploration through extensive seismic reflection surveys and drilling of numerous deep wells. In this work, geological-geophysical data from 160 deep wells drilled for hydrocarbon exploration/exploitation purposes in the Po Plain and in the facing northern Adriatic Sea have been collected and digitized along with several published geological cross-sections and maps. These data have been used to reconstruct the overall subsurface 3D architecture and to extract the physical properties of the subsurface geological units.

The digitized data are suitable to be imported into geo-software environments so to derive the geophysical-mechanical properties of the geological units for a wealth of applied and scientific studies such as geomechanical, geophysical and seismological studies.

The integrated dataset may represent a useful tool in defining regional first order strategies to ensure the safety of the urbanized areas and human activities and to reduce natural and anthropic risks that may affect this crucial region of Europe. In particular, the data collected would be useful to highlight sensible areas where data collection and more detailed studies are needed. Nowadays, such issues are particularly relevant for the underground industry development related to the increasing interest on possible CO_2 and hydrogen underground storage, which can play a fundamental role in the energy transition process towards the decarbonisation goals.

1 Introduction

35   The Po Plain in the north of Italy is the most productive and prosperous region of Italy (Fig. 1a), with a per capita income similar to that of central and northern European countries (https://ec.europa.eu/eurostat; Helliwell and Putnam, 1995; Tabellini, 2010; European Commission, 2016). The area is densely populated (https://ec.europa.eu/eurostat; Fig. 1a) and hosts numerous UNESCO world heritage sites such as the cities of Venice, Verona, Bergamo, and Ravenna (https://whc.unesco.org/; Fig. 1b). Since the second half of the 20th century, the discovery and exploitation of numerous hydrocarbon (mostly gas) resources

40   contributed to the economic development of Italy. The Po Plain and the facing northern Adriatic Sea host indeed the majority of hydrocarbon fields in the country (extracting almost 33% of the total national gas production) and most of the Italian underground gas storage sites, which have been operative since the 1960s (https://unmig.mise.gov.it/; Fig. 1b).

The Eni-Agip Company hydrocarbon exploration and exploitation activities in the Po Plain and northern Adriatic Sea led to the production of a large amount of subsurface data, which includes: (i) seismic data acquired through extensive regional 2D

45   and 3D seismic surveys for the development of onshore/offshore hydrocarbon fields and (ii) well data acquired during the drilling of explorative and development wells. The subsurface dataset provided structural, stratigraphic, and sedimentological information, which allowed the accurate knowledge of the regional subsurface architecture and geological evolution (e.g., Pieri and Groppi, 1981; Cassano et al., 1986; Casero, 2004; Ghielmi et al., 2010, 2013; Fantoni et al., 2009, 2010).

The geological evolution of the Po Plain is accompanied by seismic, subsidence and flooding events that are the main

50   phenomena to consider in natural hazards assessment. The cultural, social, and economic relevance of this region asks for a careful evaluation of both natural hazards and impact of human activities to mitigate the potential correlated risks and guarantee the safety of the urbanized areas and human activities themselves.

The Po Plain is characterized by moderate seismicity (International Commission on Hydrocarbon Exploration and Seismicity in the Emilia region, 2014). Nonetheless, instrumental and historical intermediate-strong (Mw≥5.0) earthquakes hit the area

55   (Rovida et al., 2022), such as the events occurred in 1117 (Mw 6.5; Verona area), in 1570 (Mw 5.6; Ferrara area), and 2012 when a seismic sequence in the Modena and Ferrara provinces occurred (main shock Mw 6.09). The latter event promoted the implementation of the seismic monitoring network as an essential instrument for the safe management of industrial activities. Notice that no case of anthropogenically-induced seismicity has been documented so far in the study area (Braun et al., 2020). The Po Plain is also characterized by significant subsidence of both natural and anthropic origins, particularly intense after the

60   economic growth following the World War II. The natural component is the result of several geological processes, such as sediment load and compaction, vertical tectonic movements, and rebound effects after the last deglaciation (Carminati and Di Donato, 1999). Anthropogenic subsidence is primarily influenced by groundwater withdrawal for industrial, agricultural, and civil uses (e.g., Herrera-Garcia et al., 2021). Subordinately, it is linked to hydrocarbon (mainly gas) exploitation from onshore and offshore reservoirs (Carminati and Martinelli, 2002; Bitelli et al., 2020).

65   Subsidence mainly affects the central and eastern sectors of the Po Plain: the highest total subsidence rates, greater than -60 mm/yr, were evaluated for the Bologna city area (Carminati and Martinelli, 2002; Zerbini et al., 2007; Baldi et al., 2009),

whereas the highest natural component reaches -2.0 mm/yr at the pede-Apennine zone, near the city of Bologna. The difference between the total (natural plus anthropogenic) vs natural components of the present-day subsidence shows that the main factor controlling modern subsidence in this region is anthropogenic (Carminati and Martinelli, 2002).

70   Subsidence is monitored through the implementation of different technologies (GPS, InSAR, levelling surveys) useful to prevent, mitigate, and control the natural processes as well as the human ones (e.g., Dacome et al., 2015; Benetatos et al., 2020).
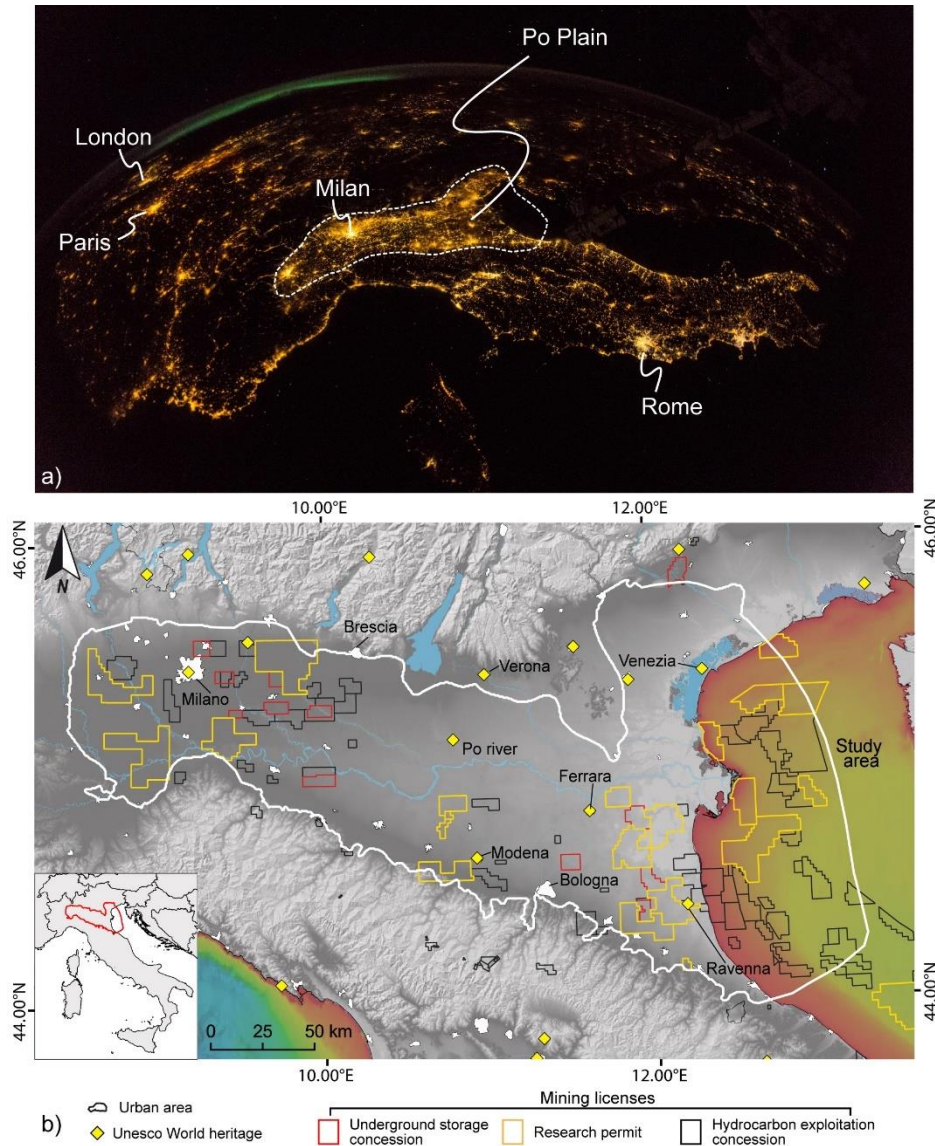
Figure 1: (a) Modified photo of the ESA astronaut Alexander Gerst, snapped from the International Space Station, that clearly
75   **reveals the high-density population in the Po Plain area highlighted by the strong night-light intensity (credit: ESA/NASA - CC BY-SA IGO 3.0; the original photo has been modified). (b) The figure shows the main cities in the Po Plain, the UNESCO world heritages (data from https://whc.unesco.org/), the current mining licenses from https://unmig.mise.gov.it/.**

Flood events related to the Po River (which crosses the whole Po Plain) and its tributaries represent an additional natural risk (Domeneghetti et al., 2015 and references therein). In the past century, the worldwide increase of flood susceptibility and risk

80   increased together with the rise of subsidence due to groundwater depletion (e.g., Herrera-Garcia et al., 2021). In the Po Plain, subsidence and flood hazards are presumably linked since there is a clear-cut correlation between high flood frequency and rapid subsidence, whereas only a few floods occurred in low subsidence areas (Carminati and Martinelli, 2002). Nevertheless, in the first half of 2022, the most significant drought since at least 70 years was observed for the area, causing extensive damage to agriculture, and encouraging the entry of the saline wedge at the mouth of the Po River along the Adriatic coast.

85   The protection of the cultural, social, and economic heritage of the Po Plain makes the adoption of all available measures necessary to reduce the impact of natural and anthropic-derived hazards in the study area.

To this end, the definition of the physical and geometrical attributes of the outcropping and subsurface geological units provides fundamental knowledge for several scientific issues and could be used in preliminary definition of engineering operations. As an example, the integration of physical parameters of subsurface geological units into a well-defined 3D model can be applied

90   to (i) reduce the uncertainties for earthquake location, contributing to the calculation of more accurate focal mechanisms and performing wave-propagation and ground-motion simulations (e.g., Magistrale et al., 1996; Süss et al., 2001; Molinari et al., 2015; Livani et al., 2022), and (ii) understand, simulate, and predict the response of the geological body to subsurface natural and anthropic processes. The latter is the case of 3D geomechanical numerical models, which represent effective tools to evaluate and predict the possible effects - both at the surface and in the subsurface - of geofluid extraction and storage, to

95   guarantee a safe management of such activities as well as to quantify and better understand the ongoing geological processes (e.g., tectonic deformation, natural subsidence, etc.; Teatini et al., 2006; Codegone et al., 2016; Benetatos et al., 2020). As an example, numerical models can play a fundamental role during the geological sequestration of CO_2 and gas storage (e.g., hydrogen as an energy carrier) in natural underground formations since they are mandatory for the optimization of the development strategies, the maximization of storage efficiency, and monitoring activities.

100   In this paper, we present an integrated database of geological-geophysical data regarding the subsurface of the Po Plain and the facing Adriatic Sea. The database provides a collection of data distinguished into primitive and derived. The primitive data consist of a detailed and accurate collection and digitization of subsurface information extracted from wells, geological cross-sections, and geological maps. The derived data are obtained from the revision and processing of the primitive ones and by gridded surfaces representing the main geological units of the Po Plain subsurface.

105   It is worth mentioning that, in the study area, the geological literature offering interpretations of the subsoil is abundant in terms of geological reconstructions. Our database represents a collection of the main published works regarding the Po Plain.Detailed studies related to specific sectors of the Po Plain might not be present in our database. Recently, other subsurface geological models have been elaborated providing several isobath maps of the Po Plain (e.g., Turrini et al., 2014; ISPRA, 2015; Molinari et al., 2015; Amadori, et al., 2019, D'Ambrogi et al., 2023). It is worth mentioning two projects: the recent

110   GO-PEG project (D'Ambrogi et al., 2023)), which provides the geometry of four stratigraphic horizons in the Po Plain area deriving from GeoMol project (http://www.geomol.eu; ISPRA, 2015; Maesano and D'Ambrogi, 2016) and GeoERA-HotLime

project (https://geoera.eu/projects/hotlime6/),and the Mambo project (Molinari et al., 2015), which covers almost the entire Po Plain. In our work, due to technical difficulties (e.g., the impossibility to precisely define the depth reported in the maps), we were not able to integrate all the previous datasets. Anyhow, where possible, we integrated the available regional geological

115 models with other primitive public data to coherently define the geometry of five surfaces of the Po Plain subsurface, which are from the oldest to the youngest: the magnetic basement top, the top of the carbonate succession, the Pliocene base, the Calabrian base, and the base of recent continental deposits. The above mentioned surfaces represent lithological boundaries rather than chronostratigraphic/formational limits, that define units that are expected to show different mechanical behaviour. Most importantly, the gridded surfaces of our dataset come with a series of detailed geophysical and geological parameters

120 extracted from the composite logs of deep wells (i.e., the primitive data). In addition to the geophysical and geological data, a statistical analysis is reported and discussed as a preliminary elaboration of the collected data.

We believe that our dataset provides an important contribution to a broad audience of policymakers and scientists to understand and evaluate geological and anthropic processes in the area, and to set secure developing strategies for correct territory management and to reduce social and economic risks in a strategic area for Italy and Europe.

125 **2 Geological setting**

The Po Plain and the facing Adriatic Sea lie on the buried sector of the Adria microplate, a promontory of the Africa plate or an independent microplate, interposed between the NE-verging northern Apennines and the S-verging Southern Alps (Fig. 2; Dercourt et al., 1986; Pieri and Groppi, 1981; Castellarin et al., 1985, 1986; Doglioni, 1993; Carminati et al., 2003; Carminati and Doglioni, 2012; Fantoni and Franciosi, 2009, 2010; Turrini et al., 2016; Pezzo et al., 2020). The development of these two

130 facing fold-and-thrust belts, connected with the broad collision of the Eurasian and African plates, led to the formation of the Po Plain basin representing the foreland/foredeep basin of both orogens. Compressional tectonics affected the area since middle Eocene time, with the development of WNW-ESE oriented thrusts in the Southern Alps followed, from Oligocene-lower Miocene onward, by the NW-SE oriented thrust system of the northern Apennines (Coward et al., 1989; Carminati and Doglioni, 2012; Carminati et al., 2012; Maesano and D'Ambrogi, 2016).

135 The structural and sedimentary framework of the area has been constrained using numerous seismic reflection profiles and deep well logs (e.g., Pieri, 1983; Cassano et al., 1986; Fantoni and Franciosi, 2010; Turrini et al., 2014; ISPRA, 2015; Livani et al., 2018; Amadori et al., 2019, D'Ambrogi et al., 2023 and reference therein).

The Apennines front is characterized by three main orogenic arcs, from West to East: Monferrato, Emilia, and Ferrara Arcs (Fig. 2a). The Southern Alps represent the non-metamorphic retrobelt of the double-verging Alpine chain and, on the western

140 side of the study area, it reaches the southernmost extent with its edge very close to the northern Apennines front (Ravaglia et al., 2006; Fantoni and Franciosi, 2010; Toscani et al., 2014; Fig. 2b). The external fronts of the two facing chains are mostly buried under a siliciclastic sequence (late Eocene-actual) consisting of syntectonic sediments and recent alluvial sediments of the Po River (Pieri and Groppi,1981; Boccaletti et al., 1985; Bigi et al., 1990; Fantoni and Franciosi, 2010; Ghielmi et al., 2010, 2013; Carminati and Doglioni, 2012; Amadori et al., 2019 and reference therein). In detail, the siliciclastic sequence

145 (Fig. 3) can be subdivided into a lower (late Eocene-early Messinian) and an upper (late Messinian to present) cycle (Ricci Lucchi, 1986). The lower cycle, primarily fed by the Alpine chain, consists of silty and shaly deposits (i.e., Gallare Marls; late Eocene-to-Miocene time), in places intercalated by or interdigitated with sandy and conglomeratic deposits (i.e., Gonfolite fm.; Oligocene time), passing upward to sandy marls (Marnoso-Arenacea fm.; Langhian-to-Messinian time), clays (i.e., Colombacci fm.; Messinian time), and evaporitic deposits (i.e., Gessoso Solfifera fm.; Messinian time). The upper cycle, fed

150 by both the northern Apennines and the southern Alps, mainly consists of marine sandy and conglomeratic formations (e.g., Sergnano Gravel, Porto Corsini, Porto Garibaldi, Santerno and Asti Sandstones; Pliocene-to-middle/late Pleistocene time) and alluvial deposits (middle/late Pleistocene-to-present; e.g., Muttoni et al., 2003; Garzanti et al., 2011; Ghielmi et al., 2010, 2013; Livani et al., 2018). South of the Po River, the continental deposits consist of alluvial fan and plain deposits embedded in clays and showing elongated shapes, whereas, to the north of the Po River, the sedimentary bodies are wider, generally

155 tabular and with minor amounts of fine-grained sediments (Ori, 1993; Amorosi and Milli, 2001). These clastic sequences are superimposed on a carbonate and marly substratum (Triassic-middle Eocene), which lies on top of the platform and continental Permian-Triassic formations, lying in turn on the Variscan crystalline basement (for more details about the carbonate sequence refers to Livani et al., 2018 and references therein). The Triassic deposits are sometimes interposed by intra-sedimentary volcanic bodies (e.g., Pieri and Groppi, 1981; Castellarin, 1985; Cassano et al., 1986; Ghielmi et al., 2010; Livani et al., 2018).

160 The Southern Alps buried front consists of a repetition of Cenozoic clastic units stacked above a regional detachment in the Marne di Gallare fm. (late Eocene) and followed at depth by deep thrust cutting the Mesozoic carbonates and the Variscan crystalline basement (Fantoni et al., 2004; Figs. 2b and 3).
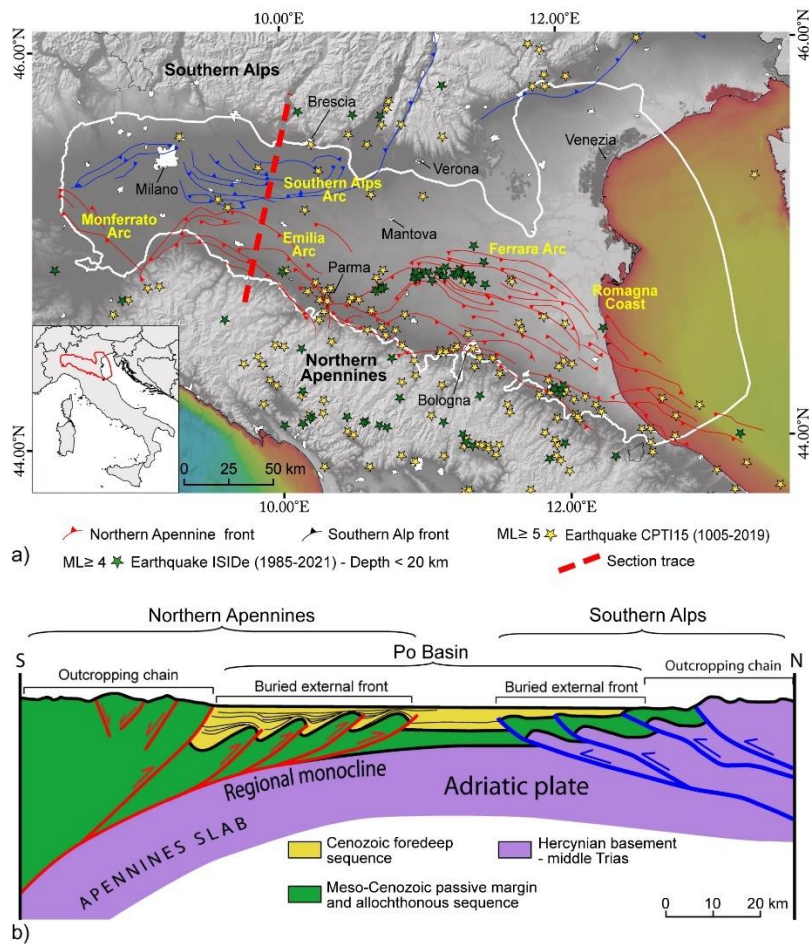
Figure 2: Study area and structural geology of the Po Plain. (a) Simplified structural map of the Po Plain (modified after Livani et al., 2018). The main buried thrusts of the northern Apennines (red colour) and Southern Alps (blue colour) fronts are shown along with the instrumental and historical seismicity (ISIDe Working Group - INGV, 2010; Rovida et al., 2022). The white polygon represents the study area. (b) Schematic geological cross-section across the Po Plain along a N-S oriented line (by Livani et al., 2018). The Northern Apennines (on the left) and Southern Alps (on the right) fronts can be identified under the Plio-Pleistocene sedimentary cover (in yellow) filling the Po Plain foredeep. Section trace is reported with a red dashed line in Fig. 2a.

The northern Apennine chain developed by off-scraping the Meso-Cenozoic sedimentary cover of the subducting Adria plate made up of siliciclastic, evaporitic, and shallow to deep-water carbonate deposits (Cati et al., 1987; Bertotti et al., 1993; Casero et al., 1990; Zappaterra, 1990; Grandić et al., 2002; Fantoni and Scotti, 2003; Fantoni and Franciosi, 2010; Masetti et al., 2012; Fig. 3).

Due to the Apennine compressional deformation, the northern Apennines thrust system migrated toward the foreland over time (among many others, Malinverno and Ryan, 1986; Doglioni, 1991; Patacca et al, 1990; Royden et al., 1988; Faccenna et al., 2003; Rosenbaum and Lister, 2004; Scrocca et al., 2006, 2007; Carminati and Doglioni, 2012 and references therein). The convergence is still active as indicated by the moderate-to-high seismicity which historically affects the Po Plain (maximum Mw between 5.5 and 6.5; Rovida et al., 2020, 2022). Studies on the active stress field in Italy (Montone et al., 2004; Devoti et

al., 2008; Cuffaro et al., 2010; Montone et al., 2012), based on the analysis of earthquake focal mechanisms, GPS records, and

180 borehole breakout data, identify active compression in the shallow portion of the Po Plain with the maximum shortening axis orthogonal to the main orogenic structures (i.e., NNE-SSW). Locally, the young land morphologies, the presence of different orders of fluvial terraces, and the deviation of some rivers (including the Po River) near the buried active tectonic structures are the tangible evidence of the recent tectonic activity (e.g., Burrato et al., 1999, 2003; Boccaletti et al., 2004a, 2004b; Wilson et al., 2009, Livio et al., 2009; Zuffetti and Bersezio, 2020; Bresciani and Perotti, 2014).
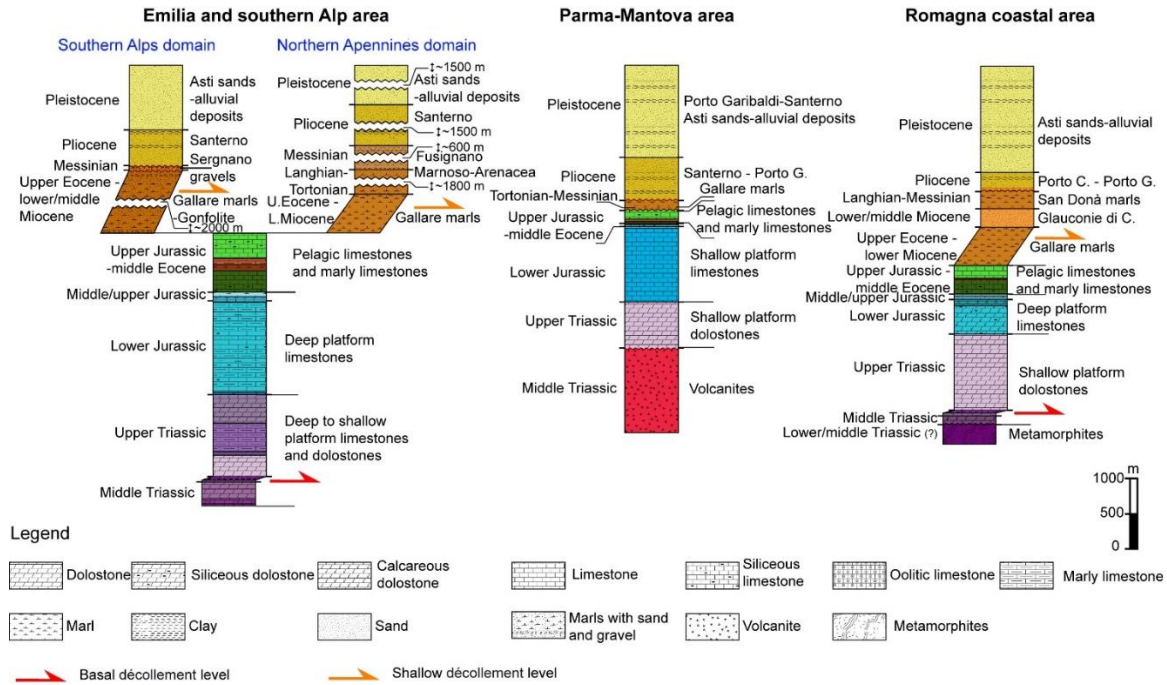
185

Figure 3: Synthetic stratigraphic columns of the Po Plain. From left to right: the stratigraphy of Emilia and Southern Alps, Parma-Mantova, and Romagna coastal areas is shown (see Fig. 2a). The carbonate passive margin (from violet to green colours) and siliciclastic active margin (from brown to light yellow colours) sequences are distinguished. The main décollement levels are highlighted (red for basal décollement and orange for shallow décollement). The stratigraphic column to the left shows the different

190 filling and the different formation thickness of the Southern Alps and the northern Apennines foredeep.

3 Database description

We realized our database by collecting, revising, and digitizing geological and geophysical data, originally in raster format, derived from public sources (i.e., databases and literature works). We collected 160 deep well composite logs, 61 published geological cross-sections, and 10 geological maps (Fig. 4; Tables 1-3). The data were georeferenced to a common geographical

195 system (WGS 84/UTM zone 32N; EPSG: 32632) by using the Open Source QGis software (version 3.12.3; http://www.qgis.org) and then uploaded into a 3D geological modelling software (Petrel® Software, version 2016.2). We organized the database into two groups, namely "primitive data" and "derived data", containing further hierarchical subdivisions created for a better organization and comprehension of the database.

The primitive data contain the product of the digitization of the collected isobath maps, the geological cross-sections, and the well data realized and acquired over a long period and for different purposes. The well data include specific sets of well logs aimed to geological/mechanical characterization of the geological units. Therefore, to achieve the integration of the different sets of data, we analysed them focusing on the stratigraphy and geological age of the interpreted units. Notice that in 2009, the Executive Committee of the International Union of Geological Sciences (IUGS) ratified a new subdivision of the Quaternary Period and the Pleistocene Epoch lowering the age of their base from the top of the Gelasian (1.8 Ma) to its base (2.58 Ma; Gibbard et al., 2010). Most of the collected data (Fig. 4; Table 1; Table 2) refer to the pre-2009 chronostratigraphic subdivisionincluding the Gelasian age in the upper Pliocene (Rio et al., 1998). On the contrary, some recent works reinterpreted the sedimentary sequence in the Po Plain and the nearby northern Adriatic Sea (e.g., Ghielmi et al., 2010, 2013; ISPRA, 2015; Maesano and D'Ambrogi, 2016; Amadori et al., 2019) using the new chronostratigraphic subdivision. In our database, since the collected primitive data (Fig. 4; Table 1; Table 2) are both prior and successive to the 2009 chronostratigraphic subdivision, we homogenized the data considering the pre-2009 Pleistocene base as Calabrian base.

We performed an accuracy analysis on the primitive data that unravelled several discrepancies in the interpretation of the subsurface geological horizons. Starting from these observations and considering the well data as the best constraint, we filtered the primitive isobath maps and the geological cross-sections to obtain a coherent dataset. The derived data consist of these filtered isobath maps and the geological cross-sections plus a series of regional surfaces of the main geological units of the Po Plain subsurface. These surfaces were generated without considering the faults occurrence/displacements and they were gridded by means of interpolation of filtered primitive data.

All data (both primitive and derived) are provided in delimited text file format organized according to the data type (i.e., well, geological cross-section, map or gridded surface).

During the processes of data collection and revision, some published subsurface data reconstruction might have not been included in the database for technical reasons such as isobath maps published at an inappropriate resolution, depth contour lines not properly stated, or geological cross-sections with a different lithostratigraphic and structural scheme compared to the one used in this work.

Figure 5 summarizes the technical procedures and the workflow used to process the data and to develop the database. In the following paragraphs, the methods and the produced primitive data are explained in detail.
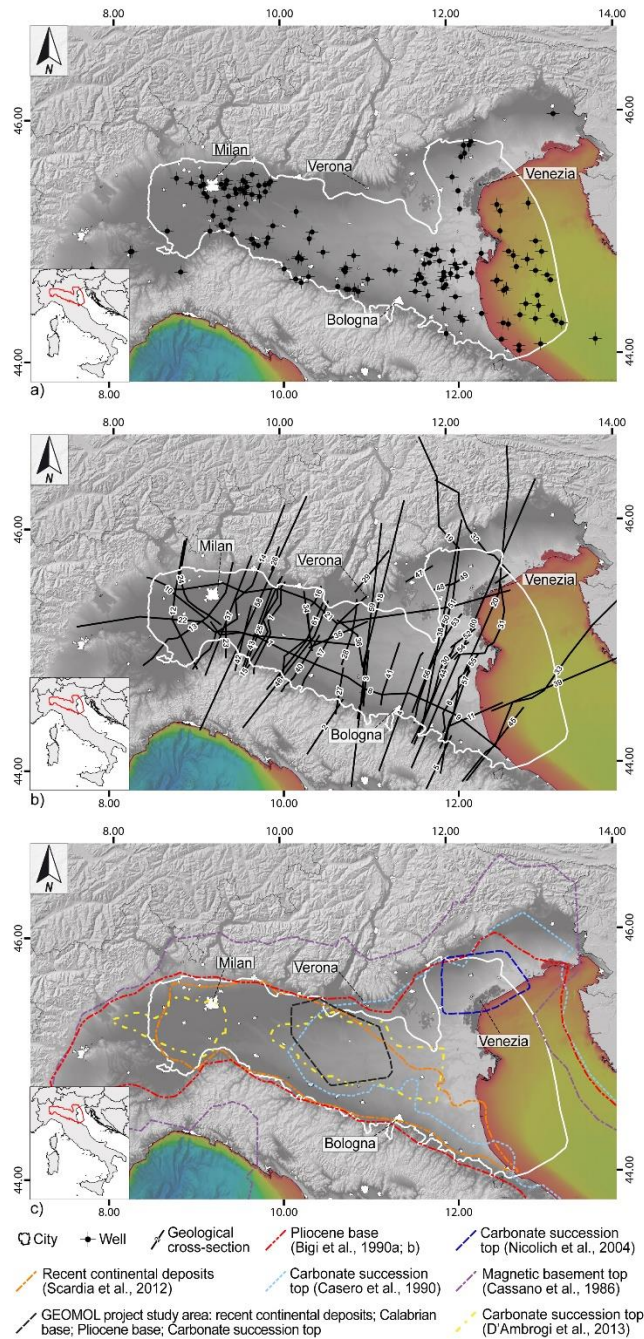
Figure 4: Primitive data collected from public sources (i.e., databases and articles from the literature). a) Location of the 160 well data collected and digitized. Some areas of the Po Plain are characterized by a low well density, hence the successive primitive data collection (i.e., geological cross-sections and maps) were focused within a slightly reduced area indicated by the white polygon. b) Traces of the geological cross-sections collected from the literature (the number on each section corresponds to a specific geological cross-section in Table 1 where the data source is specified). c) Primitive data from geological subsurface maps. The source is reported in the legend.

Table 1 – List and type of data collected for each lithological boundary.

Lithological boundary	Data source	Data type
Base of recent continental deposits	ViDEPI Project	Well tops
	Boccaletti et al., 2011	Geological cross-sections
	ISPRA, 2015	Geological cross-sections
	ISPRA, 2015	Isobath map
	Picotti et al., 2006	Geological cross-sections
	Scardia et al., 2012	Isobath map
	Wilson et al., 2009	Geological cross-sections
	Wilson et al., 2009	Geological cross-sections
Calabrian base	ViDEPI Project	Well tops
	Boccaletti et al., 2011	Geological cross-sections
	Casero, 2004;	Geological cross-sections
	Cassano et al., 1986	Geological cross-sections
	Fantoni and Franciosi, 2009	Geological cross-sections
	ISPRA, 2015	Geological cross-sections
	ISPRA, 2015	Isobath map
	Lindquist, 1999	Geological cross-sections
	Livani et al., 2018	Geological cross-sections
	Maesano et al., 2015	Geological cross-sections
	Picotti et al., 2006	Geological cross-sections
	Pola et al., 2014	Geological cross-sections
	Toscani et al., 2009	Geological cross-sections
	Turrini et al., 2015	Geological cross-sections
	Wilson et al., 2009	Geological cross-sections
Pliocene base	ViDEPI Project	Well tops
	Bigi et al., 1990	Isobath map
	Boccaletti et al., 2011	Geological cross-sections
	Casero, 2004;	Geological cross-sections
	Cassano et al., 1986	Geological cross-sections
	Fantoni & Franciosi, 2009	Geological cross-sections
	ISPRA, 2015	Geological cross-sections
	ISPRA, 2015	Isobath map
	Livani et al., 2018	Geological cross-sections
	Maesano et al., 2015	Geological cross-sections
	Picotti et al., 2006	Geological cross-sections

	Pola et al., 2014	Geological cross-sections
	Toscani et al., 2009	Geological cross-sections
	Turrini et al., 2015	Geological cross-sections
	Wilson et al., 2009	Geological cross-sections
	ViDEPI Project	Well tops
	Boccaletti et al., 2011	Geological cross-sections
	Casero, 2004;	Geological cross-sections
	Casero et al., 1990	Isobath map
	Cassano et al., 1986	Geological cross-sections
	Fantoni & Franciosi, 2009	Geological cross-sections
	D'Ambrogi et al., 2023	Isobath map
	ISPRA, 2015	Geological cross-sections
	ISPRA, 2015	Isobath map
Carbonate top	Lindquist, 1999	Geological cross-sections
	Livani et al., 2018	Geological cross-sections
	Maesano et al., 2015	Geological cross-sections
	Nicolich, 2004	Isobath map
	Picotti et al., 2006	Geological cross-sections
	Pola et al., 2014	Geological cross-sections
	Toscani et al., 2009	Geological cross-sections
	Turrini et al., 2015	Geological cross-sections
	Wilson et al., 2009	Geological cross-sections
Magnetic basement top	Cassano et al., 1986	Isobath map

Table 2 – List of the geological cross-sections collected and used to build the 3D geological model. "Section number" refers to section traces reported in Fig. 4; "Figure number" refers to the figure in the original work; "Section" refers to the number of the section in the corresponding figure of the original work, "Repositioned" indicates whether the section trace has been modified according to the intersections with data located more accurately; "Section length" represents the length in kilometres of each geological sections. The total length of the collected geological cross-sections is 6341 km.

Section number (present work)	Data source	Figure number (source work)	Section (source work)	Repositioned	Section length (km)
1		Fig. 5	A-A'		92.54
2		Fig. 5	B-B'	✓	59.3
3	Boccaletti et al., 2011	Fig. 5	C-C'		50.6
4		Fig. 5	D-D'	✓	115.35
5		Fig. 5	E-E'	✓	53.16

6		Fig. 5	F-F'	✓	63.46
7		Fig. 5	G-G'		108.46
8		Fig. 5	H-H'		102.31
9		Fig. 5	H'-H''		88.82
10	Casero, 2004	Plate 2	2a		46.11
11		Plate 3	3b	✓	97.24
12			3	✓	123.3
13			4	✓	131.36
14			5	✓	180.45
15			6	✓	103.58
16			7	✓	99.01
17	Cassano et al., 1986		8	✓	106.33
18			9	✓	205.48
19			10	✓	279.5
20			11	✓	289.43
21			12	✓	351.38
22			13	✓	267.05
23		Fig. 3	1(1)	✓	30.94
24		Fig. 3	1(2)	✓	96.03
25		Fig. 3	2(1)	✓	86.48
26		Fig. 3	2(2)	✓	21.54
27		Fig. 3	3(1)	✓	42.23
28	Fantoni and Franciosi, 2009	Fig. 3	3(2)	✓	61.17
29		Fig. 3	3(3)	✓	48.03
30		Fig. 3	4	✓	92.45
31		Fig. 3	4	✓	98.25
32		Fig. 3	4	✓	131.64
33		Fig. 3	5	✓	238.39
34			A-A'		54.11
35	ISPRA, 2015		B-B'		57.99
36			C-C'		52.23
37	Lindquist, 1999	Fig. 3a		✓	117.06

38		Fig. 3b		✓	194.67
39		Fig. 3c			131.08
40	Livani et al., 2018	Fig. 11	C-C'		62.4
41		Fig. 11	D-D'		58.78
42		Fig. 6	1		60.47
43	Maesano et al., 2015	Fig. 6	2		78.36
44		Fig. 6	3		99.78
45		Fig. 6	4		84.22
46	Picotti et al., 2007	Fig. 5	A-A'		140.53
47		Fig. 5	A-A'		27,72
48		Fig. 5	AA-AA'(1)		14.55
49		Fig. 5	AA-AA'(2)		20.09
50		Fig. 5	B-B'(1)		18.13
51	Pola et al., 2014	Fig. 5	B-B'(2)		8.21
52		Fig. 5	C-C'		27.35
53		Fig. 5	CC-CC'		29.90
54		Fig. 5	D-D'		21.10
55		Fig. 5	E-E'		22.26
56	Toscani et al., 2009	Fig. 3	A-A'	✓	67.89
57		Fig. 3	B-B'	✓	67.74
58		Fig. 7	B		235.47
59	Turrini et al., 2015	Fig. 7	C	✓	244.71
60		Fig. 7	D	✓	288.34
61	Wilson et al., 2009	Fig. 2c		✓	94.82
				Total length (km)	6341.33

Table 3 – Wells collected in the database with their location (X-coordinate and Y-coordinate) and the rotary table elevation (m a.s.l.). The coordinates of wellhead locations are reported in the geographical system used in the database (WGS 84/UTM zone 32N; EPSG: 32632). UOI: well identification number. The deepest lithology unit reached by each well corresponds to: (1) Recent continental deposits; (2) Late Pliocene-Pleistocene deposits; (3) Late Miocene-Late Pliocene deposits; (4) Early-Late Miocene deposits; (5) Triassic-Eocene carbonate units; (6) Crystalline basement.

UOI	Well name	X (Well head)	Y (Well head)	Rotary table (m a.s.l.)	Deepest lithology unit
W001	Adele 1	775896	4948539	26.0	3
W002	Adriana 1	813510	4935428	26.0	4

W003	Afrodite 1	776447	4949455	17.5	4
W004	Agnadello 1	540028	5032805	101.0	4
W005	Albertina 1	817436	4975718	12.5	4
W006	Alex 1	814736	4925902	22.0	4
W007	Alma 1	811808	4913895	12.2	3
W008	Amelia 2Bis	797531	4917463	21.2	3
W009	Anguilla 1	782121	4910090	18.3	3
W010	Antegnate 1	562955	5037036	114.0	4
W011	Antinea 1Bis	796791	4889359	18.9	5
W012	Arcade 1	750637	5073687	65.0	5
W013	Arcobaleno 1	776213	5018899	23.4	4
W014	Arese 1	504947	5044530	170.2	4
W015	Arlecchino 1	779266	5013094	24.7	4
W016	Arluno 1	495098	5038326	155.5	4
W017	Azzura 1	784981	4941745	27.0	3
W018	Baggiovara 1	645422	4940921	65.2	4
W019	Ballan 1	735056	5044275	21.4	5
W020	Bando 7	725514	4949472	5.0	4
W021	Baricella 1	702411	4949324	12.2	3
W022	Baura 001	714740	4971856	9.4	4
W023	Bedeschi 1 dir	727384	4922999	21.0	4
W024	Bedeschi 1 dirA	727384	4922999	21.0	4
W025	Belgioioso 1	523877	4998221	79.0	4
W026	Bellaria Mare 1	780580	4894982	17.6	4
W027	Berillo 1	786889	4908968	18.9	3
W028	Bertolani 1 Dir	640133	4940818	79.0	4
W029	Bevilacqua 1	677149	4958950	19.3	3
W030	Bosco Rosso 1	616314	4975044	32.5	3
W031	Brignano 2	551050	5046463	157.0	5
W032	Canopo 1	796699	4884893	19.0	5
W033	Cantoni 1	603577	4987473	36.0	4
W034	Cargnacco 1	827970	5102613	87.0	6
W035	Carmela 1	866844	4895571	27.0	2

W036	Cascina Buzzoni 1	723577	4967057	9.0	4
W037	Cascina Nuova 1 dir	701791	4976442	16.0	5
W038	Cascina San Francesco 1	737689	4963897	4.5	4
W039	Cascina San Pietro 1 dir	542559	5032244	100.0	4
W040	Case Pinelli 1	657445	4950268	34.7	4
W041	Casello 1 dir	593907	4970938	48.0	4
W042	Castano 1	481511	5043078	182.4	5
W043	Castel Gabbiano 1	557324	5036392	108.0	4
W044	Cerere 1	802948	4927606	26.0	3
W045	Cernusco 1	527759	5040908	136.0	4
W046	Cernusco 3	527060	5037627	123.0	4
W047	Chiosone 1	570184	4999305	45.8	4
W048	Cinzia 1	835893	4909975	26.0	4
W049	Claudia 1	822486	4954196	27.5	4
W050	Codevigo 1	741986	5014848	5.0	5
W051	Cona 2	709424	4964097	8.2	4
W052	Cornegliano 19	532686	5013752	89.0	4
W053	Correggio 33	636767	4957061	41.8	3
W054	Correggio 34 dir	637237	4960570	39.0	3
W055	Correggio 35 dir	637233	4960569	39.0	3
W056	Correggio 36 dir	637231	4960569	39.0	3
W057	Correggio 37 dir	637229	4960566	39.0	3
W058	Correggio 38 dir	637224	4960564	39.0	3
W059	Correggio 39 dir	637222	4960562	39.0	3
W060	Correggio 39 dirA	637222	4960562	39.0	3
W061	Correggio 40 dir	635457	4958855	41.0	3
W062	Corsico 1	506882	5029271	115.4	4
W063	Corte Mezzo 1	739452	4960575	6.0	3
W064	Corte Vittoria 1	735863	4976384	10.0	5
W065	Cusignana 1	745549	5073487	80.0	5
W066	Daniela 1	791415	4972060	25.0	4
W067	Dolo 1 dir	740530	5031608	8.0	3
W068	Fabbrico 1	644606	4971873	23.5	3

W069	Ferrara 1	714006	4965211	13.0	5
W070	Filetto 1	745087	4912388	18.0	4
W071	Filetto 1 dirA	745087	4912388	18.0	4
W072	Gallignano 2	563219	5030619	93.0	4
W073	Gandini 2 dir	544340	5029732	96.7	3
W074	Gemma 1	830405	4912198	27.5	4
W075	Ghiara 2 dir	593461	4969928	51.0	4
W076	Ginevra 1	782492	4939951	26.0	3
W077	Gisolo 1	580476	4959830	285.0	4
W078	Gladiolo 1	811922	4958195	27.0	4
W079	Glenda 1	825659	4949631	27.0	4
W080	Goro 1	761932	4974041	7.0	4
W081	Gudo Gambaredo 1 dir	509669	5025876	111.0	2
W082	Inverno 1dir	530799	5005318	84.1	4
W083	Irma 1	794204	4961737	27.0	4
W084	Isabella 1	811951	4985391	27.4	4
W085	Lanzano 1	529337	5026512	96.9	4
W086	Linarolo 1	522494	5000129	86.0	4
W087	Locate Triulzi 1	517074	5022007	103.6	3
W088	Maiero 1	727422	4956521	6.5	4
W089	Malossa 4	542687	5041078	130.4	5
W090	Malossa B Iniezione	544749	5039426	130.0	4
W091	Mariangela 1	779126	4994676	26.0	3
W092	Marrara 1	706920	4955104	18.7	4
W093	Marzeno 41	729689	4900222	177.0	5
W094	Merlengo 1	746589	5066132	48.2	4
W095	Mirazzano 1 dir	525371	5033901	114.0	3
W096	Molinella 1	710103	4946510	15.0	4
W097	Montalbano 21	704740	4954756	11.2	4
W098	Monte Acuto 1 dir	532837	4991334	79.0	4
W099	Montecchi 1	629875	4943513	101.8	4
W100	Montecchio 1	720948	4977826	8.0	4
W101	Moretta 1	385425	4956518	269.2	6

W102	Muradolo 1	565668	4988208	48.0	4
W103	Negrini 1	726897	4942291	4.2	4
W104	Nervesa 1	752475	5076899	73.5	5
W105	Nervesa 1 dirA	752475	5076899	73.5	4
W106	Novi Ligure 2	485442	4956778	192.5	3
W107	Offanengo 1	557914	5026164	86.0	3
W108	Oriana 1	827485	4916892	26.0	4
W109	Ornella 1	787040	4975930	18.9	4
W110	Paese 1 dir	743131	5062880	39.0	4
W111	Pandino 1	536388	5029141	87.0	4
W112	Pavonara 1	711695	4973319	8.0	4
W113	Portoverrara 3	727680	4952637	4.6	4
W114	Priorato 1	592876	4969565	50.0	4
W115	Priorato 2 dir	592876	4969565	50.0	3
W116	Pumenengo 1	566508	5038091	123.0	4
W117	Quarto 1	552990	4982890	89.0	4
W118	Rachele 1	805089	5020241	27.0	4
W119	Raffaella 2	804262	4968628	27.6	4
W120	Rea 1 dir	512307	4994494	73.0	5
W121	Riccardina 1	701174	4938999	25.9	4
W122	Rolassa 1	440470	4975679	156.0	4
W123	Russi 1 dir	742428	4915614	15.0	4
W124	Salerano 001	530085	5015436	83.4	4
W125	San Alessandro 1	596519	4968724	55.0	4
W126	San Alessandro 1 dirA	596519	4968724	55.0	3
W127	San Cipriano 1	545609	5019541	72.9	3
W128	San Ermelinda 1	729376	4945094	2.0	3
W129	San Genesio 1	515135	5008502	95.5	5
W130	San Michele 1	596263	4947217	241.0	4
W131	San Polo 1 dir	556581	4981094	93.0	4
W132	Sartirana 1	473042	4994514	108.0	4
W133	Scandiano 1 dirB	637657	4941105	80.2	4
W134	Scandiano 2 dir	639189	4940924	75.2	4

W135	Schiorsi 1	733784	4955454	4.3	3
W136	Segrate 1	522534	5037547	122.0	4
W137	Seniga 1	591646	5012369	56.0	3
W138	Serena 1	816551	4890738	28.6	3
W139	Seresole 1	546169	5035239	112.0	4
W140	Sermide 1	684777	4983402	16.9	3
W141	Settimo Milanese 1	503716	5035857	146.5	5
W142	Solarolo 1	606267	4993664	43.0	5
W143	Sommariva Del Bosco 1	403848	4959735	307.7	4
W144	Spada 1	682501	4959755	24.9	4
W145	Torrazza 1	762257	4918726	6.0	2
W146	Torre Del Poggio 1	550408	4986992	75.0	4
W147	Torrente Riglio 1 dir	564192	4983772	66.0	4
W148	Trava 1	739883	4952560	3.2	3
W149	Trenno 1	506511	5037331	146.0	4
W150	Trescore 1	550917	5028054	86.4	4
W151	Urago D'Oglio 1	568054	5040092	121.0	4
W152	Vaiano 1	535573	5033071	104.3	4
W153	Valgera 1	439138	4975331	131.0	4
W154	Valle Isola 1	753080	4956134	8.0	3
W155	Valletta 1 dir	712816	4935159	15.0	3
W156	Varano 1	746924	4964965	8.5	4
W157	Vigatto 10 dir	602968	4952521	132.2	4
W158	Vignola 1	717279	4977064	11.5	5
W159	Villavecchia 1 dir	591224	4950301	237.2	4
W160	Zoboli 1	648649	4938952	70.0	4
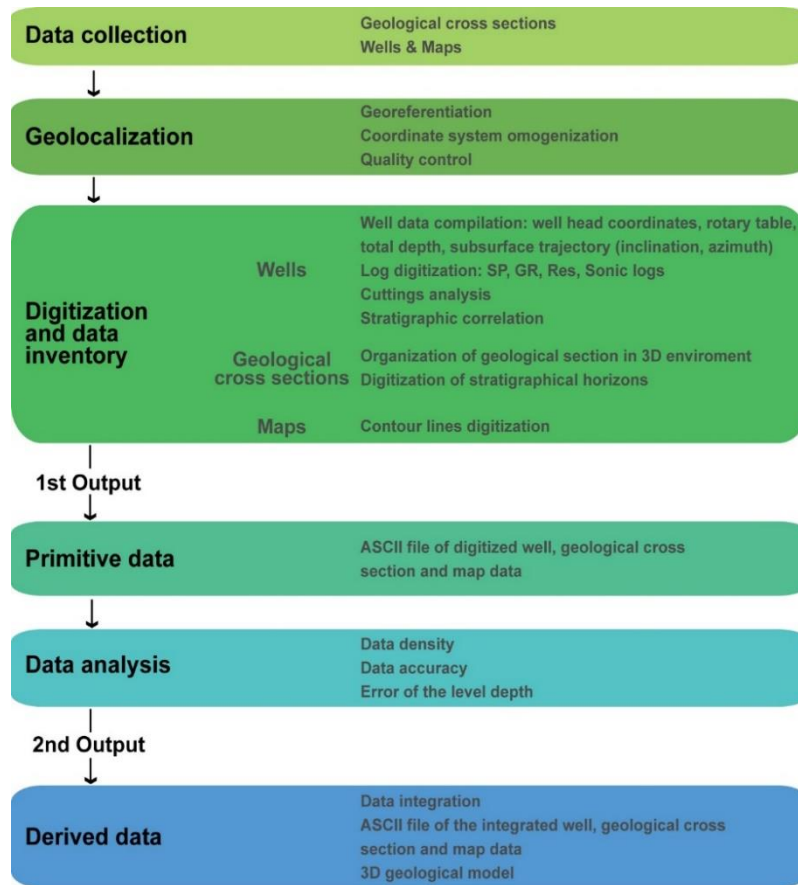
Figure 5: Workflow used for the database creation.

4 Primitive data: methods and results

Primitive data derive from the digitization of public data that have been graphically and spatially checked to eliminate errors due to low graphical quality and distortions, scale errors or bad positioning. We digitized the principal horizons reported in the geological cross-sections, the isobaths of the main geological surfaces represented in the geological maps, and the well locations comprised their trajectory along depth, lithological and stratigraphical information, and geophysical logs from well composite logs. We performed the entire workflow (data collection, image georeferencing, data quality check, integration, and model-building) by using QGis and Petrel® software. The digitized data have been then organized in text files. Further details about the data processing are given below.

4.1 Well data

The source of well data is the VIDEPI project database (http://www.videpi.com). We collected data from 160 well logs, originally in a raster format (scale 1:1000), drilled in the Po Plain and in the northern Adriatic Sea (Fig. 4). Borehole

information, such as wellhead coordinates, rotary table elevation, measured depths, true depths, total depth, and deviation survey, is indicated on the composite logs, along with lithological, stratigraphic and fluid saturation information (Fig. 6). In addition, composite logs include the Spontaneous Potential log (SP), which is used for lithological characterization and stratigraphic correlation purposes, and the Resistivity log (Res), used for the identification of hydrocarbon bearing intervals; in the more recent well master logs, the SP log is replaced by, or in certain cases complemented, a Gamma Ray log (GR). Furthermore, 133 out of 160 well composite logs of our dataset also include sonic log registrations that provide insights into sonic velocity variations with depth (Fig. 6). Further lithological information derives either from drill cuttings or from laboratory analysis of core samples collected from wells.
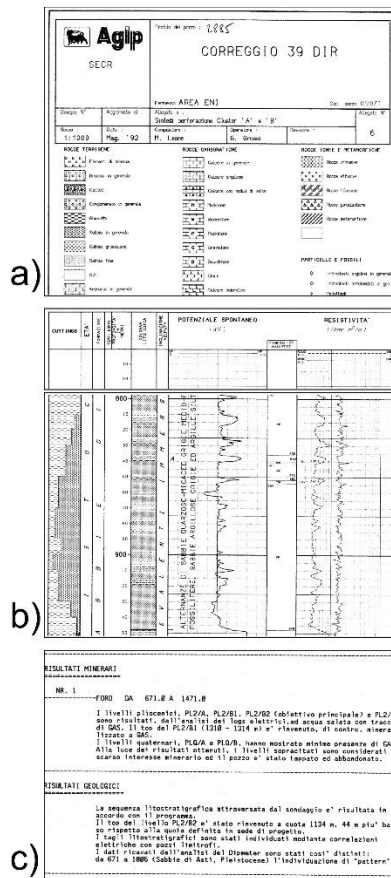
Figure 6: Typical composite log (scale 1:1000) available from the VIDEPI database (www.videpi.com), originally in .pdf format. a) Section of the well name, well coordinates information and well log legend. b) Section of the well log data, lithological cuttings and completion information. c) Notes section (e.g., well trajectory, core information, geological information, technical data).

An accurate revision of the wellhead positioning and the subsurface trajectory was necessary to properly collect and organize the well data and to furnish a dataset suitable to be imported into the most common 3D modelling software. From each well, we first transformed the reported geographic coordinates (expressed in ROMA 40 as geodetic datum) into projected

coordinates using the WEST BOAGA projection (geodetic datum: ROMA 40) and then in the geographical system used for
280   our database (i.e., WGS 84/UTM zone 32N; EPSG: 32632). Most of the wells are vertical and, hence, the well trajectory at
depth is set using the wellhead coordinates and the total depth values. On the contrary, the path of the directional wells was
reconstructed by using inclination (Inc) and azimuth (Az) information at the depth reported on the composite logs.
We then digitized the available SP log, GR log, and Sonic log of each well using the WebPlotDigitizer software (Rohatgi,
2014). Table 4 shows the log availability for each well in the project. The digitization procedure was performed manually,
285   with a variable sampling step, or by a semi-automatic method of line recognition. The digitized logs were then resampled to a
constant step of 0.5 m. Fig. 7 shows an example of the digitization process.
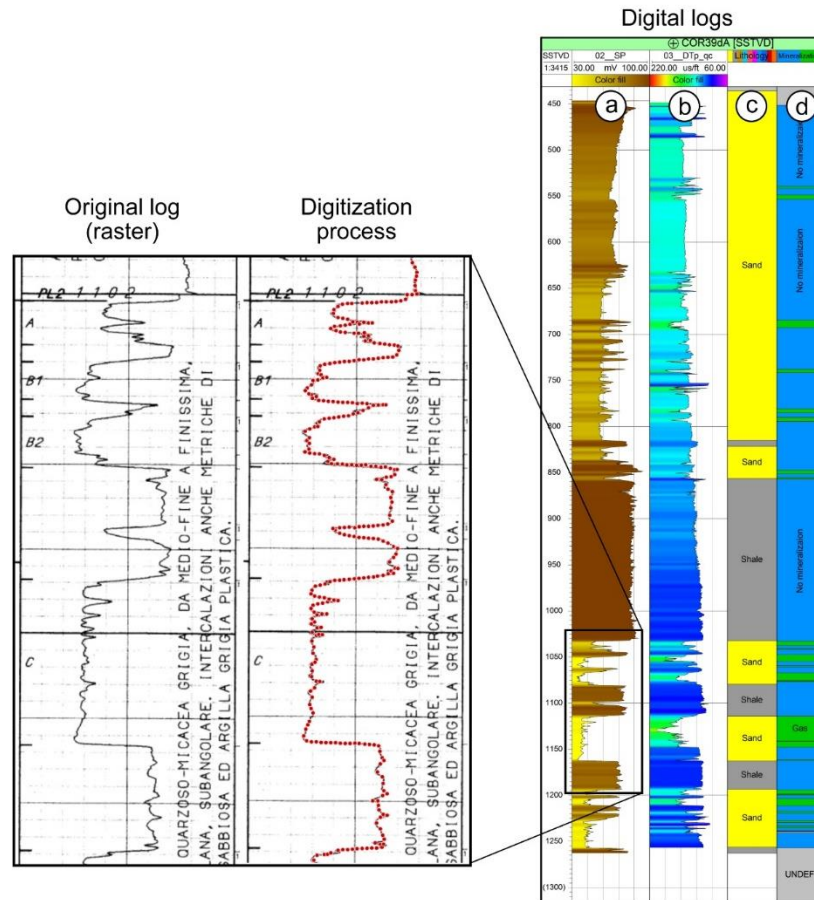
**Figure 7: Example of the digitization process for Well Correggio 39 dirA. The left panel shows the original Spontaneous Potential
log in the composite log (raster format) and the digitalized points (in red). The right panel shows the digitized (a) SP and (b) Sonic
290   logs and the classification of (c) Lithology and (d) Hydrocarbon bearing sections.**

Table 4 – List of collected wells and the relative log availability. "UOI" indicates the identification number for each well. GR:
Gamma Ray log; SP Spontaneous Potential log.

UOI	Well name	GR	Lithology	Mineralization	Sonic	SP
W001	Adele 1		✓	✓	✓	✓
W002	Adriana 1		✓	✓	✓	✓
W003	Afrodite 1		✓	✓	✓	✓
W004	Agnadello 1		✓	✓		✓
W005	Albertina 1		✓	✓	✓	✓
W006	Alex 1		✓	✓		✓
W007	Alma 1		✓	✓		✓
W008	Amelia 2Bis		✓	✓		✓
W009	Anguilla 1		✓	✓	✓	✓
W010	Antegnate 1		✓	✓		✓
W011	Antinea 1Bis		✓	✓		✓
W012	Arcade 1		✓	✓	✓	✓
W013	Arcobaleno 1	✓	✓	✓	✓	
W014	Arese 1		✓	✓		✓
W015	Arlecchino 1	✓	✓	✓	✓	
W016	Arluno 1		✓	✓		✓
W017	Azzura 1		✓	✓	✓	✓
W018	Baggiovara 1		✓	✓	✓	✓
W019	Ballan 1	✓	✓	✓	✓	
W020	Bando 7		✓	✓	✓	✓
W021	Baricella 1		✓	✓		✓
W022	Baura 001		✓	✓		✓
W023	Bedeschi 1 dir		✓	✓	✓	✓
W024	Bedeschi 1 dirA		✓	✓	✓	✓
W025	Belgoioso 1		✓	✓	✓	✓
W026	Bellaria Mare 1		✓	✓		✓
W027	Berillo 1		✓	✓	✓	✓
W028	Bertolani 1 Dir		✓	✓	✓	✓
W029	Bevilacqua 1		✓	✓	✓	✓
W030	Bosco Rosso 1		✓	✓	✓	✓
W031	Brignano 2		✓	✓	✓	✓
W032	Canopo 1		✓	✓		✓
W033	Cantoni 1		✓	✓	✓	✓
W034	Cargnacco 1		✓	✓	✓	✓
W035	Carmela 1		✓	✓	✓	✓
W036	Cascina Buzzoni 1		✓	✓	✓	

ID	Name					
W037	Cascina Nuova 1 dir		✓	✓	✓	✓
W038	Cascina San Francesco 1		✓	✓	✓	✓
W039	Cascina San Pietro 1 dir		✓	✓	✓	✓
W040	Case Pinelli 1		✓	✓	✓	✓
W041	Casello 1 dir	✓	✓	✓	✓	
W042	Castano 1	✓	✓	✓	✓	✓
W043	Castel Gabbiano 1		✓	✓	✓	✓
W044	Cerere 1		✓	✓	✓	✓
W045	Cernusco 1		✓	✓		✓
W046	Cernusco 3		✓	✓		✓
W047	Chiosone 1		✓	✓	✓	✓
W048	Cinzia 1		✓	✓	✓	✓
W049	Claudia 1		✓	✓	✓	✓
W050	Codevigo 1		✓	✓	✓	✓
W051	Cona 2		✓	✓		✓
W052	Cornegliano 19		✓	✓		✓
W053	Correggio 33		✓	✓	✓	✓
W054	Correggio 34 dir		✓	✓	✓	✓
W055	Correggio 35 dir		✓	✓	✓	✓
W056	Correggio 36 dir		✓	✓	✓	✓
W057	Correggio 37 dir		✓	✓	✓	✓
W058	Correggio 38 dir		✓	✓	✓	✓
W059	Correggio 39 dir		✓	✓	✓	✓
W060	Correggio 39 dirA		✓	✓	✓	✓
W061	Correggio 40 dir		✓	✓	✓	✓
W062	Corsico 1		✓	✓		✓
W063	Corte Mezzo 1		✓	✓	✓	✓
W064	Corte Vittoria 1	✓	✓	✓	✓	✓
W065	Cusignana 1		✓	✓	✓	✓
W066	Daniela 1		✓	✓	✓	✓
W067	Dolo 1 dir		✓	✓	✓	✓
W068	Fabbrico 1		✓	✓	✓	✓
W069	Ferrara 1		✓	✓		✓
W070	Filetto 1		✓	✓	✓	✓
W071	Filetto 1 dirA		✓	✓	✓	✓
W072	Gallignano 2		✓	✓		✓
W073	Gandini 2 dir		✓	✓	✓	✓
W074	Gemma 1		✓	✓	✓	✓
W075	Ghiara 2 dir		✓	✓	✓	✓

W076	Ginevra 1		✓	✓	✓	✓
W077	Gisolo 1		✓	✓	✓	✓
W078	Gladiolo 1		✓	✓	✓	✓
W079	Glenda 1		✓	✓	✓	✓
W080	Goro 1		✓	✓	✓	✓
W081	Gudo Gambaredo 1 dir		✓	✓	✓	✓
W082	Inverno 1dir		✓	✓	✓	
W083	Irma 1		✓	✓	✓	✓
W084	Isabella 1		✓	✓	✓	✓
W085	Lanzano 1		✓	✓		✓
W086	Linarolo 1		✓	✓	✓	✓
W087	Locate Triulzi 1		✓	✓		✓
W088	Maiero 1		✓	✓		✓
W089	Malossa 4	✓	✓	✓		✓
W090	Malossa B Iniezione		✓	✓	✓	✓
W091	Mariangela 1		✓	✓	✓	✓
W092	Marrara 1		✓	✓		✓
W093	Marzeno 41		✓	✓	✓	✓
W094	Merlengo 1	✓	✓	✓	✓	
W095	Mirazzano 1 dir		✓	✓	✓	✓
W096	Molinella 1		✓	✓	✓	✓
W097	Montalbano 21		✓	✓		✓
W098	Monte Acuto 1 dir		✓	✓	✓	✓
W099	Montecchi 1		✓	✓	✓	✓
W100	Montecchio 1		✓	✓	✓	✓
W101	Moretta 1		✓	✓	✓	✓
W102	Muradolo 1		✓	✓	✓	✓
W103	Negrini 1		✓	✓	✓	✓
W104	Nervesa 1	✓	✓	✓	✓	
W105	Nervesa 1 dirA	✓	✓	✓	✓	
W106	Novi Ligure 2		✓	✓	✓	✓
W107	Offanengo 1		✓	✓	✓	✓
W108	Oriana 1		✓	✓	✓	✓
W109	Ornella 1		✓	✓	✓	✓
W110	Paese 1 dir	✓	✓	✓	✓	
W111	Pandino 1		✓	✓		✓
W112	Pavonara 1		✓	✓	✓	✓
W113	Portoverrara 3		✓	✓		✓
W114	Priorato 1		✓	✓	✓	✓

ID	Name					
W115	Priorato 2 dir		✓	✓	✓	✓
W116	Pumenengo 1		✓	✓	✓	✓
W117	Quarto 1	✓	✓	✓	✓	
W118	Rachele 1		✓	✓	✓	✓
W119	Raffaella 2		✓	✓	✓	✓
W120	Rea 1 dir		✓	✓	✓	✓
W121	Riccardina 1		✓	✓	✓	✓
W122	Rolassa 1		✓	✓	✓	✓
W123	Russi 1 dir		✓	✓	✓	✓
W124	Salerano 001		✓	✓		✓
W125	San Alessandro 1		✓	✓	✓	✓
W126	San Alessandro 1 dirA		✓	✓	✓	✓
W127	San Cipriano 1		✓	✓		✓
W128	San Ermelinda 1		✓	✓	✓	✓
W129	San Genesio 1	✓	✓	✓	✓	✓
W130	San Michele 1		✓	✓	✓	✓
W131	San Polo 1 dir		✓	✓	✓	✓
W132	Sartirana 1		✓	✓	✓	✓
W133	Scandiano 1 dirB		✓	✓	✓	✓
W134	Scandiano 2 dir		✓	✓	✓	✓
W135	Schiorsi 1		✓	✓	✓	✓
W136	Segrate 1		✓	✓		✓
W137	Seniga 1		✓	✓	✓	✓
W138	Serena 1		✓	✓	✓	✓
W139	Seresole 1		✓	✓	✓	✓
W140	Sermide 1		✓	✓	✓	✓
W141	Settimo Milanese 1		✓	✓	✓	✓
W142	Solarolo 1		✓	✓	✓	✓
W143	Sommariva Del Bosco 1	✓	✓	✓	✓	✓
W144	Spada 1		✓	✓		✓
W145	Torrazza 1	✓	✓	✓	✓	✓
W146	Torre Del Poggio 1		✓	✓	✓	✓
W147	Torrente Riglio 1 dir		✓	✓	✓	✓
W148	Trava 1		✓	✓	✓	
W149	Trenno 1	✓	✓	✓		✓
W150	Trescore 1		✓	✓		✓
W151	Urago D'Oglio 1		✓	✓	✓	✓
W152	Vaiano 1		✓	✓	✓	✓
W153	Valgera 1		✓	✓	✓	✓

W154	Valle Isola 1	✓	✓	✓	✓
W155	Valletta 1 dir	✓	✓	✓	✓
W156	Varano 1	✓	✓		✓
W157	Vigatto 10 dir	✓	✓	✓	✓
W158	Vignola 1	✓	✓	✓	✓
W159	Villavecchia 1 dir	✓	✓	✓	✓
W160	Zoboli 1	✓	✓	✓	✓

The Resistivity log (Res) was used to identify the mineralized intervals of wells with gas bearing layers and then to create a new "discrete" type of log with indications regarding "hydrocarbon bearing" and "water bearing" layers. Subsequently, Res was used to isolate and remove the sonic log measurements for those geological intervals affected by the hydrocarbon presence (Figs. 7 and 8).
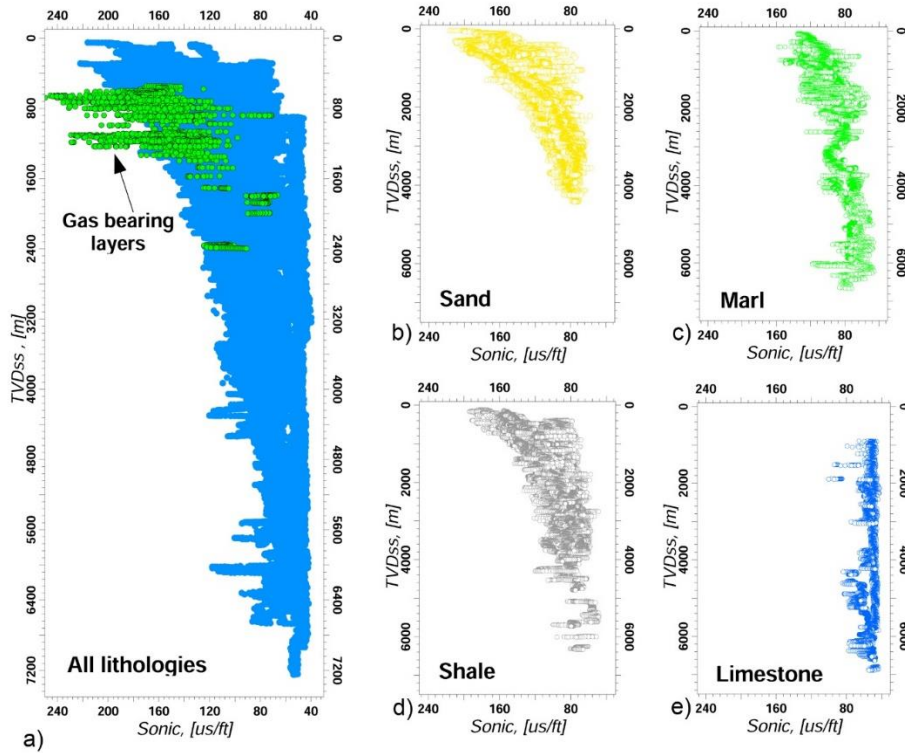
Figure 8: a) Variation of transit time with depth for all samples showing the effect of the presence of gas. b-e) Variation of transit time with depth for the sand, marl, shale, and limestone lithologies, respectively.

The stratigraphic information on the composite logs together with SP and GR logs was used to perform a correlation at the
305 regional scale by identifying those units showing different lithological properties and defining surfaces dividing geological
successions with different mechanical properties. . The main units recognized include (from youngest to oldest):

- Recent clastic deposits of the Po Plain and the Adriatic Sea, consisting of gravels and sands of continental
environment identified from the cuttings of the first tens to hundreds of meters for each well. This unit has been
widely analysed in the literature (Regione Emilia Romagna & ENI-AGIP, 1998; Regione Lombardia & ENI-
310 AGIP, 2002; Scardia et al., 2012; Ghielmi et al., 2013).
- Late Pliocene-Pleistocene sand-rich sequences, consisting of sands and clayey sands with clayey interlayers of deep
marine to continental environment (Sabbie di Asti Group), connected to the latest filling of the Po Plain foredeep.
- Late Miocene-late Pliocene clastic deposits connected to the evolution of the northern Apennine foredeep and top-
thrust basins, including:
315 i. clay-rich units made up of variably silty clays with minor sand (Argille del Santerno Fm.);
ii. sand-rich (mostly foredeep turbiditic) units made up of thick sand beds with minor clay and thin-bedded
sand-clay repetitions (e.g., Marnoso-Arenacea Fm., Bagnolo Fm., Fusignano Fm., Caviaga Fm., Porto
Garibaldi Fm., Porto Corsini Fm.);
iii. conglomeratic units made up of shallow-marine and fluvio-deltaic conglomerates and sands with minor clay
320 (e.g., Sergnano Fm., Cortemaggiore Fm., Boreca Conglomerate).
- Early-late Miocene marly sequences, consisting of marl, clayey marl, clay and sandy marl with sand intercalations
recording deposition on the foreland ramp (e.g., Marne di Gallare Group).
- Triassic to Eocene undifferentiated carbonate units consisting of prevailing limestone (mainly mudstone and
packstone-grainstone) and dolomite with subordinate marl.
325 - Variscan crystalline basement.

We collected additional data related to the lithological characteristics of the subsurface sedimentary units from cuttings
description. The cuttings description contains the information collected during mud logging, where rock fragments from the
borehole reach the surface due to the circulation of the drilling fluids. Those data were combined with the SP and GR logs and
with lithological data from core sample analysis reported in the well profile to characterize the lithology of the entire well. In
330 total, we identified 9 macro-lithologies listed below together with the descriptions commonly found in the well profiles:

- Gravel (e.g., polygenic gravel, gravel prevalent, polygenic gravel and sand with shale interbeds, gravel and pebbles
with sand interbeds).
- Sand (e.g., sand, sand prevalent, shaly sand, fine sand, sand with shale interbeds, sand and shaly sands, sand banks).
- Cemented Sand (e.g., cemented sand, fine-grained cemented sand, cemented sand and pebbles, calcareous cemented
335 sand, sand of variable cementation).
- Shale (e.g., shale, silty shale, gray shale, marl shale, prevalent shale).
- Sand/shale alternances (e.g., gray shales and sand, shales with sand interbeds).

- Conglomerates (e.g., polygenic conglomerate, polygenic conglomerate with shale, polygenic conglomerate with sand interbeds).

340   - Marl (e.g., marls, silty marls, gray silty marls, marls and sandy marls, grey marls with cemented sand).

- Dolomite (e.g., dolomite, calcareous dolomite, crystalline dolomite, shaly dolomite, gray dolomite).

- Limestone (mudstone/wackestone/packstone/grainstone).

Well data represent the main constrain for the subsequent 3D geological modelling phase. As shown in Figure 4, the distribution of the wells in the area is not homogeneous and some regions are characterized by low well density. For this

345 reason, the collection of the other primitive data (i.e., geological cross-sections and maps) was focused in the area indicated by the white polygon in Figure 4, excluding the most isolated wells.

We performed a preliminary analysis of the sonic velocity variations with depth using the collected data and the newly created lithological and mineralization logs (Fig. 8). The sonic logs display transit time values in the range 40-140 μsec/ft. However, we observed even higher values (approx. 150-200 μsec/ft) in shallow formation that were concentrated to the first tens to few

350 hundred meters from the surface and are mostly connected to gravel lithologies that are characterized by poor consolidation (Fig. 8). In some cases, unusually high or low sonic log values with respect to the general data trend for a certain lithology can be ascribed to the presence of thin layers with different lithological characteristics, to possible borehole damage or to the presence of fractures. The currently available information does not allow a clear interpretation of their causes and even their removal. Most of the lithologies show a gradual decrease in transit time with increasing depth (Fig. 8b-d) and, at about 4 km

355 depth, the transit time flattens out showing rather constant values for higher depths, independently from the lithology. The continuous decrease of the P-waves transit time with depth reflects the increasing compaction of the sediments due to the overburden weight. The limestone is an exception, showing a relatively constant transit time independently of the depth. The presence of gas significantly increases the transit time with respect to water-saturated rocks: the so-called "gas effect" outlines as a rock density reduction (Fig. 8a).

360 The abundance of each lithology within the main units, defined in this study, significantly affects the average mechanical rock properties of the entire unit (Fig. S2). One of the advantages of the analysis performed is the possibility to assign specific mechanical properties for each lithology and for different depths. Knowing the amount of each lithology present in the geological units we can achieve a more precise characterization of the subsurface geological layers that is fundamental for improving the quality of the geomechanical simulations. Applications of the sonic log analysis in defining mechanical rock

365 properties of the subsurface of the Po Plain area can be found in Benetatos et al. (2023a, 2023b). In the first work the authors propose a workflow for geomechanical simulations through seabed monitoring. A significant step in the workflow involves the rock mechanical characterization that is performed through the analysis of the sonic log data that are converted to dynamic Young's modulus values specific for the different lithologies and for various depths. The same approach is also followed by Benetatos et al.(2023b) to calculate mechanical properties of the Argille del Santerno Fm.. They used well log data and

370 compared them to those derived from laboratory analysis of core samples. This comparative analysis revealed relations

between well log and laboratory derived properties and contributed to the understanding of the deformation behaviour of this important geological formation that extends across northern Italy.

4.2 Geological cross-sections

We collected 6341 km of published geological cross-sections (Cassano et al., 1986; Lindquist, 1999; Casero, 2004; Picotti et
375 al., 2006; Fantoni and Franciosi, 2009; Toscani et al., 2009; Wilson et al., 2009; Boccaletti et al., 2011; Pola et al., 2014; ISPRA, 2015; Maesano et al., 2015; Turrini et al., 2015; Livani et al., 2018; Table 1). Several procedures were implemented for uploading, calibrating, and revising the geological cross-sections in a 3D environment and, finally, for digitizing the selected horizons. The location maps (i.e., maps displaying the section traces) and the cross-sections were graphically re-arranged and improved to reduce imperfections and errors due to the low quality and/or images distortion. We then
380 georeferenced the location maps in QGis environment digitizing the relative section traces (Fig. 4). Based on the geographically oriented section traces, the cross-section images (raster format) were properly uploaded in a 3D environment. The geological cross-sections composed of segments with different orientations were cut into several parts and separately imported. Where necessary (i.e., location inconsistency), the geological cross-sections were repositioned using the intersections with other data such as wells, surface geology (e.g., geological boundaries, faults, etc.), other geological cross-sections, and orographic and
385 hydrographic features (e.g., rivers).

The revised and georeferenced cross-sections were finally uploaded into a 3D project in the Petrel® software. We digitized four geological horizons that roughly correspond to the boundaries of the main lithological discontinuities recognized through the well data analysis. The horizons are, from the oldest to the youngest: the top of the carbonate succession (which becomes more marly in its upper portion) dividing a mainly carbonate succession (below) by a mainly siliciclastic succession (above)
390 and it does not represent a chronostratigraphic boundary, the Pliocene base, the Calabrian base, and the base of recent continental deposits. In the regions characterized by a vertical duplication of the same unit due to the effect of thrusting, we digitized the hanging wall of the units until the hanging wall cut-off, then passing directly to the footwall of the same unit. In such a way, a marked artificial step was generated; however, we deem this approximation as necessary for the successive 3D modelling dataset creation, which does not integrate any fault element. In the data collection process, some public geological
395 cross-sections were excluded from the database and the digitization process. For instance, the AGIP geological cross-sections reported on the Italian geological maps at 1:100,000 scale (sheets 75, 77 and 88; https://www.isprambiente.gov.it/it/attivita/suolo-e-territorio/cartografia/carte-geologiche-e-geotematiche/carta-geologica-alla-scala-1-a-100000) were not used due to the geological interpretation based on scarce deep data information (many deep wells and seismic reflection profiles were unavailable at that time), strongly differing from interpretations recently proposed
400 on the basis of a large amount of subsoil data. Furthermore, some vintage sections (i.e., Bally et al., 1986) were excluded since some more recent geological cross-sections passing close to their traces show a more precise localization and better graphical properties allowing a more accurate digitization process.

For each digitized horizon a delimited text file in ASCII format reporting the xyz coordinates is generated. Since the digitization process was performed manually, the data are provided with an irregular sampling step.

4.3 Geological maps

The 3D database also includes data derived from 10 published subsurface geological maps. We digitized the following maps:

- 2 isobath maps of the base of the recent continental deposits (QC1 horizon map by ISPRA, 2015; Scardia et al., 2012);
- 1 isobath map of the Calabrian base (QM1 horizon map by ISPRA, 2015);
- 2 isobath maps of the Pliocene base (Bigi et al., 1990a, 1990b; ISPRA, 2015);
- 4 isobath maps of the carbonate succession top (Casero et al., 1990; Nicolich, 2004; ISPRA, 2015; D'Ambrogi et al., 2023);
- 1 isobath map of the magnetic basement top (Cassano et al., 1986).

The maps, available in hard copy and/or in raster format, were graphically revised and re-arranged in order to reduce possible scanning defects and distortions. The maps were then georeferenced, and the contour lines digitized by using QGis software. The digitized contour lines were exported and uploaded into the 3D Petrel® database. We then verified in a 3D environment their consistency with other subsurface geological information, especially from well data.

For each map, a delimited text file in ASCII format reporting the xyz coordinates of the contour lines was generated. Since the digitization process was performed manually, the data are provided with an irregular sampling step.

5 Data accuracy

A widespread accepted standard approach to address map accuracy is still not available. Recent studies suggest methods and standards for error analysis of geological or subsurface maps (e.g., Kint et al., 2020 and references therein). However, these methods are still affected by significant bias as they depend on the data availability and the criteria of data selection. Quality flagging is the basic approach used to quantify uncertainty within a spatial dataset and is done by assessing metadata fields. This method can be limited to indicate the presence or absence of data or be very complex producing a full range of quantitative error ranges (e.g., Bardossy and Fodor, 2001). Kint et al. (2020) presented an approach to assess data uncertainty for a well dataset in the Quaternary succession of the Belgian Continental Shelf. They produced confidence maps based on datasets from different origins and time periods. Their method consists in: i) determination of the data density (how much data contribute to each grid cell to provide information on lateral and depth variability); ii) direct mapping of measured errors and accuracies; iii) transformation of the measured values or categorical quality flags into uncertainty percentages; iv) selection of data subsets based on the uncertainty maps. Not all these points are always feasible or necessary. This renders the method non-general. For example, in the case of few data or datasets without associated uncertainty, steps ii) and iv) are not recommended/feasible.

Furthermore, the uncertainty drags errors due to instrumental (absolute accuracy, positioning accuracy) and human (expert judgment, data selection, data origin and representation) accuracy are not often quantifiable.

435   The only "universal" and "dataset unrelated" rule when considering the geographic space comes from the first law of geography (Tobler, 1970) that states: "everything is related to everything else, but near things are more related than distant things." This law is the foundation of the concepts of spatial dependence and spatial auto-correlation and is used specifically for the inverse distance weighting method for spatial interpolation (Shepard, 1968).

Generalizing the approach proposed by Kint et al. (2020) with application to arbitrary spatial data and using the Inverse
440   Distance Weight (IDW) for our analysis, we implemented, in a preliminary way, a method to weight the accuracy/confidence of geological surfaces. For each horizon we quantified: i) the data density contributing to assess the lateral accuracy and the depth variability, ii) the accuracy based on the data density and spatial autocorrelation converted into a probability (Inverse Distance Weight - IDW) describing the confidence on the data at each point of the study area and iii) the error associated with the depth of the geological surfaces due to discrepancies between the data of different origins where different guesses exist.

445   Hence, for each point of the study area, we provided a value indicating the accuracy and a value indicating the estimated error of the depth of the geological surface.

To apply our model, we started by edging the study area including the observation region and covering it through an evaluation grid (Fig. 9a). In surface and subsurface mapping, the observations come from properly identified sites. Locations of these sites (hereafter checkpoints) are known and tag the observations. The variable of interest (i.e., horizon depth) exists in every
450   point of the region (i.e., grid nodes) but is observed only in a finite set of locations (checkpoints). The variability model describes how uncertainties increase moving away from the checkpoint with respect to the best guess, built according to the observations and the geological constraints. In our case study, the properly identified sites are points (wells), lines (the traces of geological cross-sections digitized at discrete points), and polygons (here intended as raster fields digitized at discrete points, i.e., isobaths of geological maps). Note that not all kinds of checkpoints can be considered at the same level of confidence
455   since well data give better depth-constraints to those derived by geological cross-sections or interpolated maps. For this reason, it is convenient to assign higher specific weight to first-order checkpoints (well data in our case) with respect to higher order checkpoints (sections or maps). Once the hierarchical subdivision has been made, the inverse distance (ID) principle is used to model the uncertainties at each point of the study area (i.e., at grid nodes) based on spatial autocorrelation with respect to checkpoints as:

460   $$ID = \frac{1}{1 + r^p}$$

where ID is the inverse distance, r is the distance between the point of observation and the checkpoint and p is the checkpoint order; in this study p=1 for well data, p=2 for sections, and p=3 for maps. The inverse distance (ID) is than normalized to obtain the inverse distance weight IDW as:

$$IDW = \frac{ID - ID_{min}}{ID_{max} - ID_{min}}$$

465   The *IDW* assigns a confidence based on distance autocorrelation that decreases more gently when considering first order checkpoints (red curve goes under 0.2 at 7 km of distance; Fig. 9b) with respect to higher order checkpoints (green and black curves goes under 0.2 at 2 km of distance; Fig. 9b). The total weight calculated at each point of the study area is the mean value of the weights calculated with respect to different order checkpoints. This means that *IDW*=1 is the best guess assigned to grid nodes that, in the ideal case, lie - at the same time - over checkpoints of order 1 to n (i.e., in our case over a well crossed

470   by a section and coinciding with an interpolation point of the map). Statistics of the dataset are reported in Table 5.
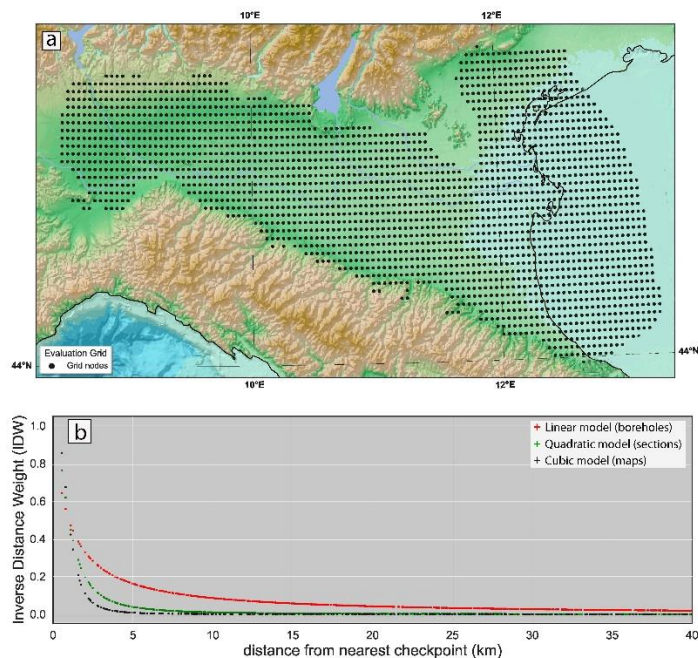
Figure 9: a) Grid-nodes used to evaluate the data accuracy and uncertainties for geological surfaces presented for the study area. At each node, based on spatial autocorrelation, we calculated the Inverse Distance Weight (IDW) with respect to points observation
475   **(checkpoints). b) The model adopted for the IDW describes how uncertainties increase moving away from the best guess at checkpoints (i.e., at well, along geologic cross-sections or on depth maps); at the same distance from a checkpoint, well data gives higher IDWs (red points) with respect to data derived from geological cross-sections or interpolated maps (green and black points).**

5.1 Data density

Four out of the five processed geological surfaces (i.e., the base of recent continental deposits, the Calabrian base, the Pliocene
480   base and the Carbonate succession top) were reconstructed using checkpoints of order 1 (i.e., well data), 2 (i.e., geological cross-sections) and 3 (i.e., subsurface geological maps). The reconstruction of the magnetic basement top derives from a unique source (Cassano et al., 1986) and, for this reason, we avoided to include this surface in the data accuracy analysis.

The analysis of our dataset (Table 5) shows that the three shallowest surfaces (i.e., recent continental deposits, Pleistocene, and Pliocene bases) are the most constrained with up to 139 checkpoints of the first order, whereas the Carbonate succession

485 top is constrained by few checkpoints of order 1. The carbonate succession top and the Pliocene base are described by the highest amount of data with a density larger than 15 total checkpoints to each grid cell.

Table 5 – Parameters of each unit. Checkpoint refers to the number of locations where the data are observed. P is the checkpoint order where p=1 for well data, p=2 for sections, and p=3 for maps.

Lithological surface	Grid points	n. checkpoints (p1)	n. checkpoints (p2)	n. checkpoints (p3)	n. checkpoints (total – Pts. Density)
Recent continental deposits base	2566	42	634	3082	3758 – 1.46
Calabrian base	2566	139	3065	2299	5503 – 2.14
Pliocene base	2566	114	3895	29795	33804 – 13.17
Carbonate top	2566	17	3309	169785	173111 – 67.46

490

5.2 Data analysis

The total number of checkpoints does not always increase the confidence level of the data. In fact, for the Calabrian base, the Pliocene base, and the Carbonate succession top, the *IDW* values also increase up to double when calculated considering checkpoints of all orders, whereas they decrease for recent continental deposits (dashed lines in Fig. 10). In the latter case,
495 higher confidence is obtained when considering only the order 1 checkpoints (solid lines in Fig. 10). The best-constrained surface is confirmed to be the Pliocene base with a high number of both well data (i.e., order 1 checkpoints) and total data. The spatial distribution of the *IDW* for the proposed surfaces is reported in Fig. 11 and represents the confidence on the variable of interest (level depth) at each node of the grid (1 = max confidence). All the maps show maximum *IDW* ≈0.7 and a mean value of 0.06 (recent continental deposits – Fig. 11a), 0.09 (Calabrian base – Fig. 11b), 0.14 (Pliocene base – Fig. 11c) and
500 0.08 (Carbonate Top – Fig. 11d). The *IDW* values indicate that the Pliocene surface has a confidence level almost double than that obtained for the other surfaces on average. Interactive figures (html format to be opened in a web browser) of each map reported in Figure 11 are available in the supplementary material (S1.zip) and provide detailed statistical information at each node of the interpolation grid.

505
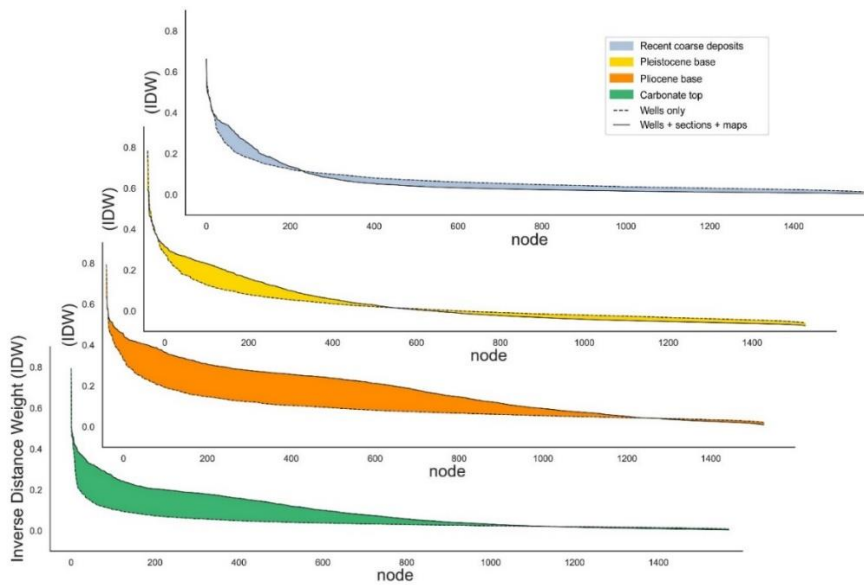
Figure 10: IDW values at grid nodes calculated for each surface considering distances from well data only (dashed lines) or integrating distances from well data plus geological cross-section plus geological maps (solid lines). The area between the two lines for each proposed surface is larger for greater uncertainties. Note that the uncertainties increase with the depth of the surfaces and that the total number of checkpoints does not always increase the confidence level of the data (as for example in the recent continental deposits).

5.3 Uncertainty associated with depth

The four surfaces analysed in this work derive from different origins and types of data (see section 3; only the magnetic basement top derives from a unique source). The variability in quality, periods of creation, owners, and compiler sensibility (human error) of the datasets produces large – not quantifiable – uncertainty affecting the input data. Furthermore, since most of the collected public data derive from interpretations of seismic profiles, the data in depth are strongly influenced by the velocity model used for the depth conversion. Unfortunately, most of the primary data are not provided along with the used velocity model and for this reason it was not possible to take into account this variable. Further, the study area is non-uniformly described by the dataset.

Each grid node is associated with one to four values of depth depending on the number of available identified sites (i.e., checkpoints from different sources) coinciding with that node. Hence, it turns out that it is possible to calculate the maximum and minimum depth of each surface at each node if at least two depth values are available in that specific node. . The range of depths at the nodes represents the uncertainty on the level description. Figure 12 shows the depth variation for the four surfaces calculated considering the maximum and minimum values for each node with at least two values . The bottoms of recent continental deposits (light blue band) and of Pleistocene unit (yellow band) show a small variation in depth (<2 km), with respect to the Pliocene (orange band - up to 6 km) and Carbonate (green band - up to 8 km) bases. Maps in Figure 13 illustrate the geographic distribution of depth evaluation uncertainty. Interactive figures of each map reported in Figure 13 are available in the supplementary material (S1.zip).
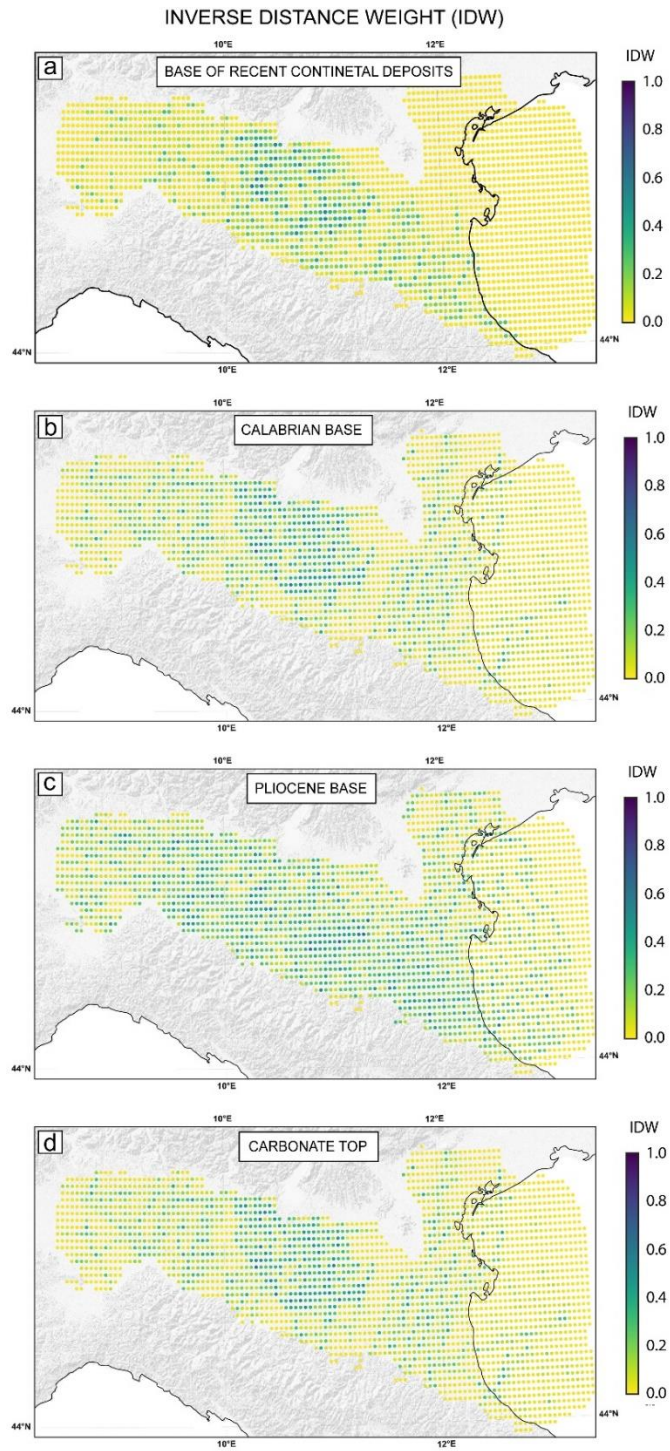
Figure 11: The spatial distribution of the IDW for the four analysed surfaces The IDW values represent the confidence on the variable of interest (level depth) at each node of the grid (1 = max confidence).
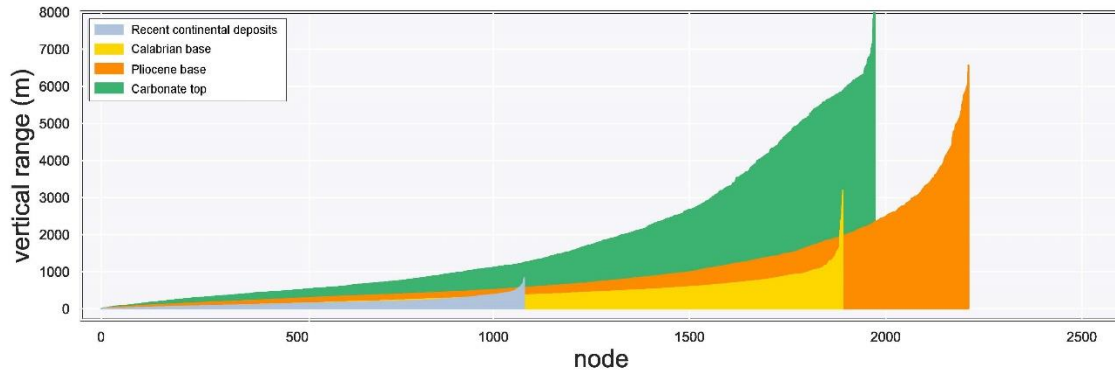
535 **Figure 12: Range of depths variation interpolated at each point of the evaluation grid based on the different datasets available for the four surfaces.**
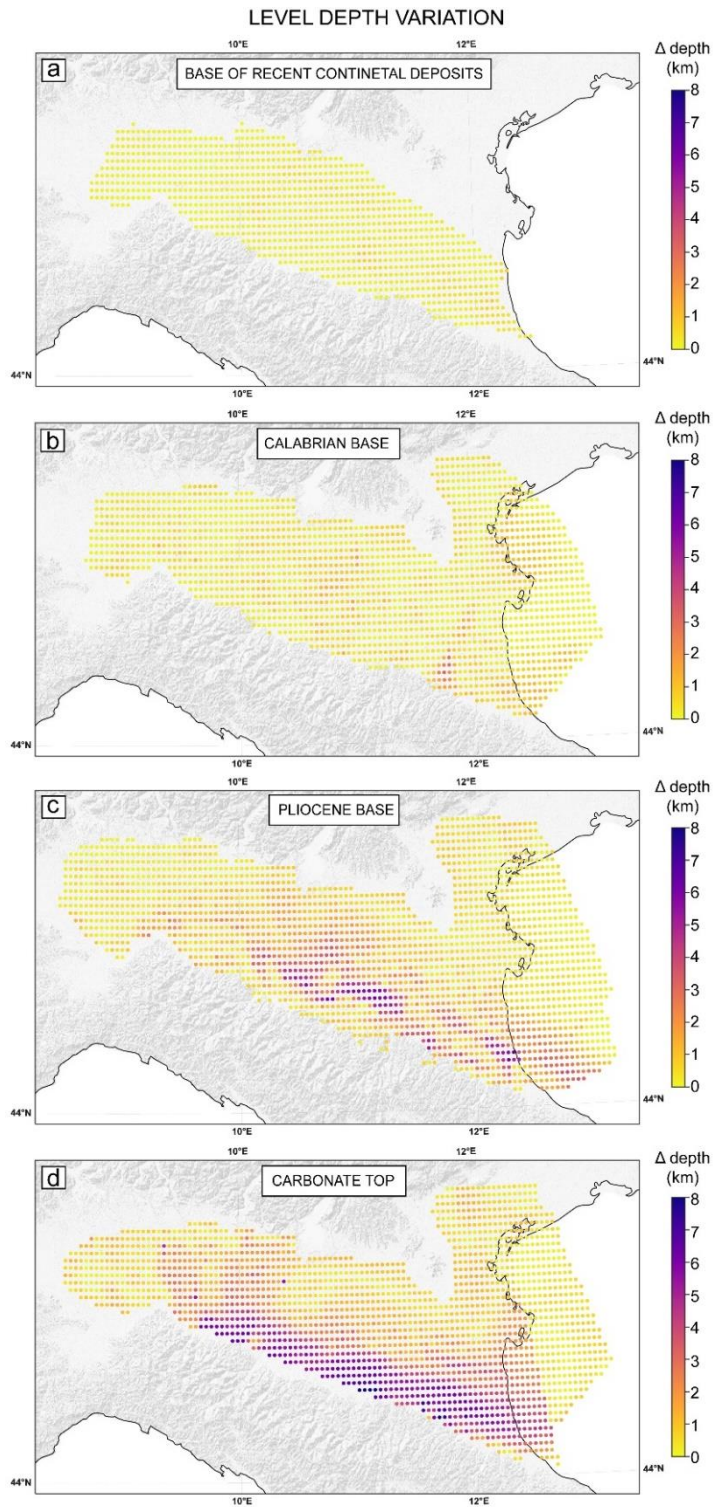
Figure 13: Geographic distribution of the range of depths variation for the four analysed surfaces

6 Derived data: methods and results

The construction of an accurate 3D geological model requires good coverage and consistency of the source data. Improving the multi-source data consistency helps to avoid errors and distortions during the 3D model generation. To ensure the most significant data coverage and consistency in the area, we revised, compared, and finally integrated the collected primitive data (i.e., wells, geological cross-sections, and maps).

Based on the data accuracy analysis and the uncertainty associated with level depth (see sections 5), we totally or partially removed the digitized primitive data showing the highest discrepancy with other data. For this purpose, as mentioned in the previous section, we assigned a priority order to the data according to their type. The highest priority is attributed to well data as they give the best depth constraint of the units (order 1 checkpoints). Hence, the well data represent the main control points of our model and none of them were excluded during the integration process. Regarding geological cross-sections and maps, if a difference in the depth of the surface is observed (Fig. 13), we kept those data showing the best fit with well data. In other cases, we kept the most recent data, except when they were very discordant from the average data (for example geological sections with a horizon depth very different from that indicated by other more reliable data) or from the predominant interpretative schemes (for example geological cross-sections with a tectonic style completely different from the preponderant interpretations). In particular, it should be pointed out that the base of recent continental deposits is defined from well data and the isobath map reported in Scardia et al. (2012) which integrates the aquifer data of the Lombardy (Regione Lombarida ENI-AGIP, 2002) and the Emilia Romagna Regions (Regione Emilia Romagna & ENI-AGIP, 1998). The inconsistent data removal was performed manually. These revised data integrated with the top of the magnetic basement, the only unit deriving from a single source (i.e., Cassano et al., 1986) and hence without any integration, were collected in ASCII format reporting the xyz coordinates of the digitized data.

We eventually constructed a 3D geological model of the rock volume interposed between the magnetic basement top and the topographic surface (Middle Triassic-present day) by means of the revised primitive data. To define the top of the modelled rock volume, since our study area is located both offshore and onshore (Fig. 2), we joined the land topography, deriving from a public digital elevation model of the whole Italian territory at an original resolution of 10 meters cell size (Tarquini et al., 2007), with the bathymetry of the offshore area (https://www.gebco.net/). The 3D geological model is made up of unfaulted surfaces obtained by gridding the revised and integrated multi-source primitive data. For the gridding process, we applied in Petrel® software a convergent interpolation algorithm with a 250 m sampling step. After gridding, we quality-checked and, where necessary, manually improved the modelled surfaces. The 3D model does not integrate any fault element. Thus, the modelled surfaces do not show any dislocation but sudden height differences in correspondence of the major tectonic structures, mostly where thrust sheets produce the vertical superimposition of the same unit (Fig. 14). The accuracy of the derived geological surfaces mainly depends on the quality and the quantity of source data (i.e., primitive data).

The aforementioned gridded surfaces represent the main boundaries that define units with different mechanical behaviour and subdivide the model into five sub-volumes, from top to bottom: the continental portion of the Quaternary deposits, the

Pleistocene Asti sands, the Pliocene sands (i.e., Santerno, Porto Corsini and Porto Garibaldi sandstones), the upper Eocene-to-Messinian siliciclastic formations (i.e., Gonfolite-Gallare Marls, Marnoso Arenacea Fm., San Donà Marls, Glauconie di Cavanella Fm., Fusignano Fm., Sergnano gravels, etc.) and the carbonate-marly succession.

The base of the recent continental deposits (Fig. 14a) was reconstructed in a restricted area, where it was intercepted by wells and modelled in the literature (Scardia et al, 2012). Areas with recent prodelta, delta and marine sediments have been excluded (Fig. 14a). The base of the recent continental deposits consists of a slightly articulated surface that generally deepens from the peripheral sectors of the model area to the median areas of the Po valley. It is characterized by a depocenter area located between the Emilia and Ferrara Arcs, where it reaches its maximum depth in the Parma area. The accuracy of this surface is generally intermediate with a strong constrain given by the isobath map digitized from Scardia et al. (2012) (Fig. 4).

The Calabrian base (Fig. 14b) generally delimits the lower contact between the Asti sands and the Gelasian and Pliocene sandstones, except where, due to the erosion affecting the anticline culminations (in correspondence with Emilia and Ferrara Arcs), the Pleistocene deposits are unconformably in contact with the Miocene ones (on the top of the Emilia Arc anticlines). This surface progressively deepens from the model borders to the inner part of the Po Plain, except for the Ferrara Arc area, where some culminations can be observed. It reaches its maximum depth in the Parma-Mantova area, and in the coastal and northern Adriatic areas. The accuracy of this surface is variable, but generally well-constrained by most of the available geological cross-sections and numerous wells. Moreover, in the Brescia-Mantova area, it is constrained by an accurate depth contour map (ISPRA, 2015; Fig. 4c).

The Pliocene base covers almost the entire area except for the Emilia and Ferrara anticlines where it was eroded due to the tectonic uplift (Fig. 14c). This lithological boundary shows a rather articulated morphology characterized by pronounced culmination (located on the main anticline axes of the Emilia and the Ferrara Arcs) and depocenter areas (between the Emilia and Ferrara Arcs, immediately south of the Ferrara Arc, and in the coastal area). The accuracy of this surface is variable but it is generally constrained by a large number of wells, geological cross-sections, and by two subsurface geological maps covering the entire model area (Bigi et al.,1990a, 1990b) and the GEOMOL project study area (ISPRA, 2015; Fig. 4c).

The Carbonate succession top separates the siliciclastic formations (upper Eocene-Present) from the carbonate and marly ones (Triassic to middle-upper Eocene in age). This surface deepens from NE to SW (beneath the northern Apennine front), with a local and pronounced elevation at the Ferrara Arc, where carbonates were markedly uplifted by the Apennine orogenic process (Fig. 14d). The accuracy of this surface is variable. It is constrained by several geological cross-sections but, due to its considerable depth, by few deep well data, mostly located on the anticline culminations. Three geological maps located in the eastern portion of the model (Casero et al., 1990; Nicolich et al., 2004) and in the central portion (D'Ambrogi et al., 2023) constrain the surface of the carbonate succession top (Fig. 4c).

As mentioned above, the gridded magnetic basement top (Fig. 14e) is based on the published depth contour map by Cassano et al. (1986), consequently, its accurateness depends only on the source data accuracy.
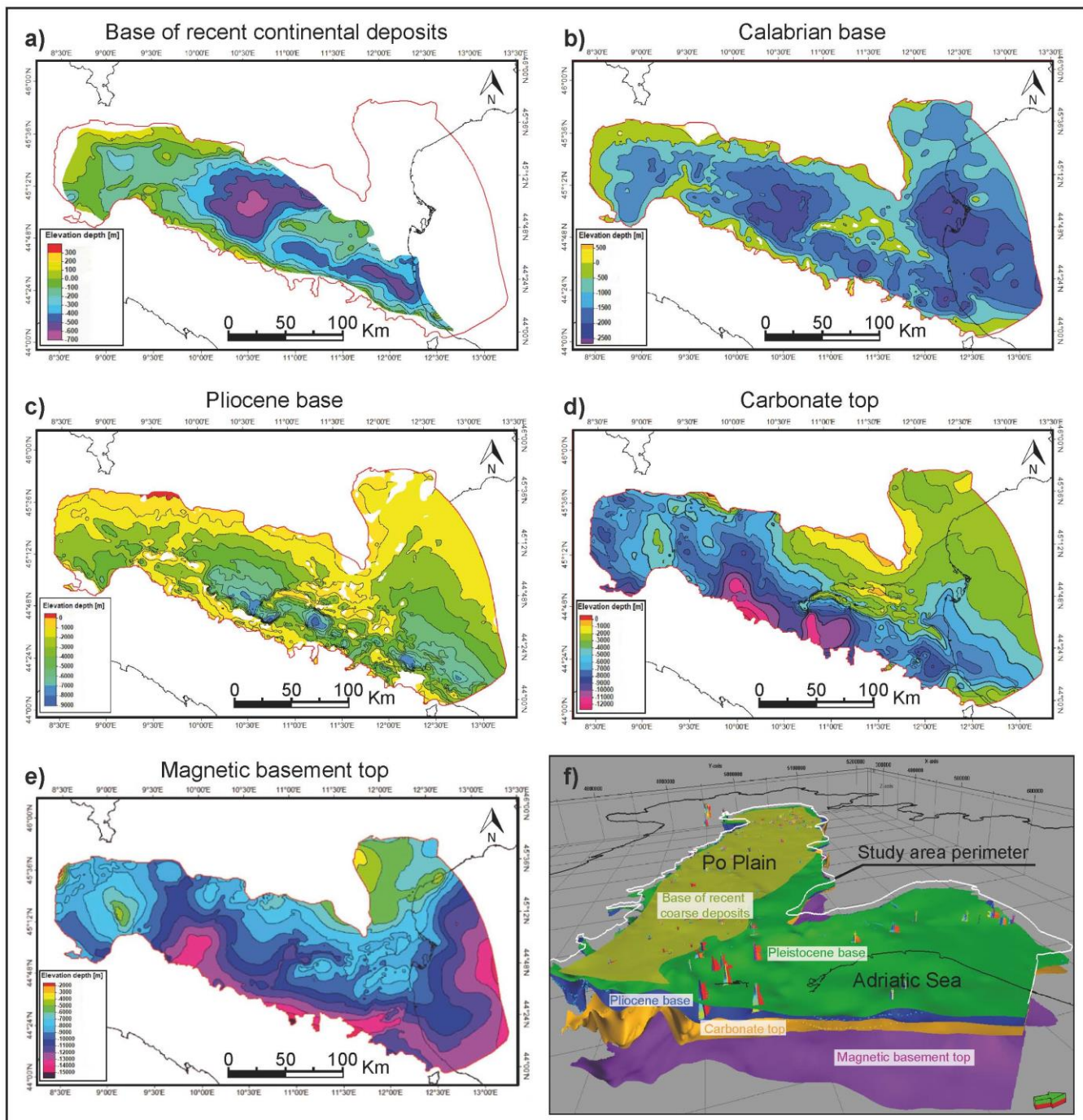
Figure 14: a-e) Geological maps representing the gridded surfaces generated with the revised primitive data: a) Base of the recent continental deposits; b) Calabrian base; c) Pliocene base; d) Carbonate succession top; e) Magnetic basement top. f) Example of the data digitized and the geological model in 3D view cut along a SW-NE oriented section.

7 Data availability

Primitive and derived data are available for open access in ASCII format at the following link: doi.org/10.5281/zenodo.8126519 (Livani et al., 2023). The format and the organization of data are explained in the related description file.

The dataset can be imported into any software handling 3D geological data, well data information and spatial vector data formats.

8 Conclusions

The database provides a collection of geological-geophysical data of the Po Plain subsurface and of the northern Adriatic Sea collected and digitized from the literature and from open repositories. We digitized data from the composite logs of 160 wells drilled in the area. Borehole information (i.e., wellhead coordinates, rotary table elevation, measured depth, true depth, total depth and deviation survey) and Spontaneous Potential, Gamma Ray, and Sonic logs are provided in ASCII format. Five horizons were digitized from 61 geological cross-sections and from 10 geological maps, from the oldest to the youngest: the top of the magnetic basement, the top of the carbonate succession, the base of the Pliocene, the base of the early Pleistocene (i.e., near top Gelasian; see section 3) and the base of recent continental deposits. The digitized data are provided in ASCII format reporting the xyz coordinates of the digitized surfaces.

Through an accuracy analysis performed on the primitive data and their subsequent processing, a new set of data has been created (i.e., derived data). Since the primary data show a depth uncertainty, we accurately revised the primary data by integrating only the data showing the best fitting. From these data, we generated a simplified 3D geological model characterized by several gridded surfaces of the main geological units (Fig. 14f).

Through the elaboration of the digitized logs is possible to directly extract geophysical and mechanical properties of the rock volume interposed between the gridded surfaces (e.g., P-wave velocity) and obtain further derived. For example, sonic velocities can be converted to mechanical rock properties, such as Young's modulus or Poisson ratio, that find applicability in geomechanical simulations which are performed to evaluate the ground subsidence/uplift phenomena (Carminati and Di Donato, 1999; Benetatos et al., 2017; Antoncecchi et al., 2021) or the change of stress field in a specific area in response to natural processes or anthropic activities (e.g., Schutjens et al., 2010; Radwan and Sen, 2021; Hemami et al., 2021; Sangnimnuan et al., 2021).

The dataset developed in the present work supports application in a wide range of research areas with benefits for scientists, practitioners, and decision-makers. As an example, once populated with the values of seismic velocity, the 3D geological model can find several applications in seismological studies. It can be used to improve the procedure and reduce the uncertainties during earthquake location, contribute to the calculation of more accurate focal mechanisms and perform wave-propagation and ground-motion simulations (e.g., Magistrale et al., 1996; Süss et al., 2001; Molinari et al., 2015; Livani et al., 2022). The 3D model also represents a starting model in perturbation studies, such as linearized inversions of travel times for

crustal velocities (e.g., Magistrale and Day, 1999) or for studies related to the seismic waveforms for crustal structure and,

645 moreover, it can be used to derive densities and compare them to gravity observations (Roy and Clayton, 1999).

In conclusion, this database will be useful to better define and mitigate the possible natural and anthropogenic risks to preserve the environment and safeguard the social and economic interests of the territory contributing to a better and more efficient management of subsoil resources.

650 **Author contribution**

Michele Livani: data curation, formal analysis, investigation, methodology, validation, visualization, writing – original draft preparation; Lorenzo Petracchini: conceptualization, data curation, methodology, project administration, supervision, validation, visualization, writing – original draft preparation; Christoforos Benetatos: conceptualization, data curation, formal analysis, investigation, methodology, supervision, validation, visualization, writing – original draft preparation; Francesco

655 Marzano: data curation, formal analysis, methodology, investigation, writing – review & editing; Andrea Billi: conceptualization, project administration, supervision, methodology, writing – review & editing; Eugenio Carminati: conceptualization, project administration, supervision, writing – review & editing; Carlo Doglioni: project administration, supervision, writing – review & editing; Patrizio Petricca: data curation, formal analysis, validation, visualization, writing – original draft preparation; Roberta Maffucci: data curation, formal analysis, investigation, validation, writing – review &

660 editing; Giulia Codegone: data curation, formal analysis, investigation, writing – review & editing; Vera Rocca: conceptualization, supervision, writing – review & editing; Francesca Verga: conceptualization, project administration, supervision, writing – review & editing; Ilaria Antoncecchi: supervision, writing – review & editing

Declaration of competing interest

665 The authors declare that they have no known competing interests.

Acknowledgments

The authors acknowledge the General Direction for Infrastructure and Safety of the Ministry for Ecologic Transition (formerly Italian Economic Development Ministry) for their support to this research.

670 **References**

Amadori, C., Toscani, G., Di Giulio, A., Maesano, F.E., D'Ambrogi, C., Ghielmi, M., and Fantoni, R.: From cylindrical to non-cylindrical foreland basin: Pliocene–Pleistocene evolution of the Po Plain–Northern Adriatic basin (Italy), Basin Res., 31, 991–1015, https://doi.org/10.1111/bre.12369, 2019.

Amorosi, A. and Milli, S.: Late quaternary depositional architecture of Po and Tevere River deltas (Italy) and worldwide

675 comparison with coeval deltaic successions, Sediment. Geol., 144, 357–375, https://doi.org/10.1016/S0037-0738(01)00129-4, 2001.

Antoncecchi, I., Ciccone, F., Rossi, G., Agate, G., Colucci, F., Moia, F., Manzo, M., Lanari, R., Bonano, M., De Luca, C., Calabres, L., Perini, L., Severi, P., Pezzo, G., Macini, P., Benetatos, C., Rocca, V., Carminati, E., Billi, A., and Petracchini, L.: Soil deformation analysis through fluid-dynamic modelling and DInSAR measurements: a focus on groundwater

680 withdrawal in the Ravenna area (Italy), BGTA-Bollettino di Geofisica Teorica ed Applicata, https://doi.org/10.4430/bgta0350, 2021.

Argnani, A., Barbacini, G., Bernini, M., Camurri, F., Ghielmi, M., Papani, G., Rizzini, F., Rogledi, S., and Torelli, L.: Gravity tectonics driven by Quaternary uplift in the Northern Apennines: insights from the La Spezia-Reggio Emilia geo-transect, quarter. Int., 101–102, 13–26, 2003.

685 Artoni, A., Rizzini, F., Roveri, M., Gennari, R., Manzi V., Papani, G., and Bernini, M.: Tectonic and climatic controls on sedimentation in Late Miocene Cortemaggior Wedge-Top Basin (Northwestern Apennines, Italy), In: LACOMBE, O., LAV, J., ROURE, F., and VERGS, J.: Thrust Belts and Foreland Basins, Springer, 431-456, 2007.

Baldi, P., Casula, G., Cenni, N., Loddo, F., and Pesci, A.: GPS-based monitoring of land subsidence in the Po Plain (Northern Italy), Earth Planet. Sc. Lett., 288(1-2), 204-212, https://doi.org/10.1016/j.epsl.2009.09.023, 2009.

690 Bally, A.W., Burbi, L., Cooper, C., and Ghelardoni, R.: Balanced sections and seismic reflection profiles across the Central Apennines, Mem. Soc. Geol. It., 35, 257-310, 1986.

Bardossy, G. and Fodor, J.: Traditional and new ways to handle uncertainty in geology, Nat. Resour. Res., 10(3), 179-187, 2001.

Benetatos, C., Codegone, G., Deangeli, C., Giani, G., Gotta, A., Marzano, F., Rocca, V., and Verga, F.: Guidelines for the

695 study of subsidence triggered by hydrocarbon production, Geoingegneria Ambientale e Mineraria, 152(3), 85-96, ISSN: 11219041, 2017.

Benetatos, C., Codegone, G., Ferraro, C., Mantegazzi, A., Rocca, V., Tango, G., and Trillo, F.: Multidisciplinary analysis of ground movements: an Underground Gas Storage case study. Remote Sensing, 12, 3487; doi:10.3390/rs12213487, 2020.

Benetatos, C., Catania, F., Giglio, G., Pirri, C.F., Raeli, A., Scaltrito, L., Serazio, C., Verga, F.: Workflow for the Validation

700 of Geomechanical Simulations through Seabed Monitoring for Offshore Underground Activities. J. Mar. Sci. Eng. 2023, 11, 1387. https://doi.org/10.3390/jmse11071387, 2023a.

Benetatos, C., Rocca, V., Verga, F., Adinolfi, L., Marzano, F.: Deformation behavior of a regional shale formation from integrated laboratory and well data analysis: Insights for underground fluid storage in northern Italy, Geoenergy Science and Engineering,, 212109, https://doi.org/10.1016/j.geoen.2023.212109. (2023b).

705 Bertotti, G., Picotti, V., Bernoulli, D., and Castellarin, A.: From rifting to drifting: Tectonic evolution of the south-Alpine upper crust from the Triassic to the Early Cretaceous, Sedim. Geol., 86(1-2), 53–76, https://doi.org/10.1016/0037-0738(93)90133-P, 1993.

Bigi, G., Castellarin, A., Coli, M., Dal Piaz, G. V., Sartori, R., Scandone, P., and Vai, G. B.: Structural Model of Italy scale 1:500.000, sheet 1. C.N.R., Progetto Finalizzato Geodinamica, SELCA Firenze, 1990a.

710 Bigi, G., Castellarin, A., Coli, M., Dal Piaz, G. V., and Vai, G. B.: Structural Model of Italy scale 1:500.000, sheet 2. C.N.R., Progetto Finalizzato Geodinamica, SELCA Firenze, 1990b.

Bitelli, G., Bonsignore, F., Del Conte, S., Franci, F., Lambertini, A., Novali, F., Severi, P., and Vittuari, L.: Updating the subsidence map of Emilia-Romagna region (Italy) by integration of SAR interferometry and GNSS time series: The 2011–2016 period. Proc. IAHS 2020, 382, 39–44, https://doi.org/10.5194/piahs-382-39-2020, 2020.

715 Boccaletti, M., Coli, M., Eva, C., Ferrari, G., Giglia, G., Lazzarotto, A., Merlanti, F., Nicolich, R., Papani, G., and Postpischl, D.: Considerations on the seismotectonics of the northem Apennines, Tectonophysics, 117, 7- 38, 1985.

Boccaletti, M., Bonini, M., Corti, G., Gasperini, P., Martelli, L., Piccardi, L., Tanini, C., and Vannucci, G.: Active structures of the emilia-romagna, GNGTS – Atti del 23° Convegno Nazionale / 02.11, 2004a.

Boccaletti, M., Bonini, M., Corti, G., Gasperini, P., Martelli, L., Piccardi, L. P., Severi, P, and Vannucci, G.: Carta
720 sismotettonica della regione Emilia-Romagna. Scala 1:250.000, Note Illustrative, Serv. Geol. Sismico e dei Suoli, Reg. Emilia Romagna, SELCA-Firenze, 2004b.

Boccaletti, M., Corti, G. and Martelli, L.: Recent and active tectonics of the external zone of the Northern Apennines (Italy), International Journal of Earth Sciences, 100(6), 1331–1348, https://doi.org/10.1007/s00531-010-0545-y, 2011.

Braun, T., Danesi, S., and Morelli, A.: Application of monitoring guidelines to induced seismicity in Italy. J Seismol (2020)
725 24:1015–1028, https://doi.org/10.1007/s10950-019-09901-7, 2020.

Bresciani, I., and Perotti, C. R.: An active deformation structure in the Po Plain (N Italy): The Romanengo anticline. Tectonics, 33(10), 2059-2076, https://doi.org/10.1002/2013TC003422, 2014.

Burrato, P., Ciucci, F., and Valensise, G.: Un approccio geomorfologico per la prima individuazione di strutture potenzialmente sismogenetiche nella Pianura Padana, Atti 18° Convegno Nazionale di Geofisica- ING, Roma, 1999.

730 Burrato, P., Ciucci, F., and Valensise, G.: An inventory of river anomalies in the Po Plain, Northern Italy: evidence for active blind thrust faulting, Ann. Geophys., 46 (5), 865-882, 2003.

Carminati, E. and Di Donato, G.: Separating natural and anthropogenic vertical movements in fast subsiding areas: the Po plain (N. Italy) case, Geophys. Res. Lett., 26(15), 2291-2294, 1999.

Carminati, E. and Martinelli, G.: Subsidence rates in the Po Plain, northern Italy: The relative impact of natural and
735 anthropogenic causation, Eng. Geol., 66, 241-255, 2002.

Carminati, E., Doglioni, C., and Scrocca, D.: Apennines subduction-related subsidence of Venice (Italy), Geophys. Res. Lett., 30(13), 1717, doi:10.1029/2003GL017001, 2003.

Carminati, E., Scrocca, D., and Doglioni, C.: Compaction-induced stress variations with depth in an active anticline: Northern Apennines, Italy, J. geophys. Res., 115, B02401, doi:10.1029/2009JB006395, 2010.

740 Carminati, E. and Doglioni, C.: Alps vs. Apennines: The paradigm of a tectonically asymmetric Earth, Earth-Science Reviews, 112, 67–96, 2012.

Carminati, E., Lustrino, M., and Doglioni, C.: Geodynamic evolution of the central and western Mediterranean: Tectonics vs. igneous petrology constraints, Tectonophysics, 579, 173–192. https://doi.org/10.1016/j.tecto.2012.01.026, 2012

Casero, P., Rigamonti, A., and Iocca, M.: Paleogeographic relationships during Cretaceous between the Northern Adriatic area and the eastern Southern Alps, Mem. Soc. Geol. Ital. 45, 807-814, 1990.

Casero, P.: Structural setting of petroleum exploration plays in Italy, in: Crescenti, U., d'Offizi, S., Merlino, S. and Sacchi L. (Eds.), Geology of Italy. Special publication of the Italian geological society for the IGC 32nd, Florence, 189– 199, 2004.

Cassano, E., Anelli, A., Fichera, R., and Cappelli, V.: Pianura Padana: interpretazione integrata di dati geologici e geofisici, Atti del 73°Congresso della Società Geologica Italiana, Roma, 1986.

Castellarin, A., Eva, C., Ciglia, G., and Vai, G. B.: Analisi strutturale del Fronte Appenninico Padano, Giornale di Geologia, 47(1-2), 47-75, 1985.

Castellarin, A. and Vai, G. B.: Southalpine versus Po plain apenninic arcs, in: Wezel, C. (Ed.): The origin of Arcs. Development in Geotectonics, 21, Elsevier, Amsterdam, 253-280, 1986.

Cati, A., Sartorio, D., and Venturini, S.: Carbonate platforms in the subsurface of the northern Adriatic Sea, Mem. Soc. Geol. It., 40, 295–308, 1987.

Codegone, G., Rocca, V., Verga, F., and Coti, C.: Subsidence Modeling Validation Through Back Analysis for an Italian Gas Storage Field. Geotech. Geol. Eng., 34, 1749–1763, https://doi.org/10.1007/s10706-016-9986-9, 2016.

Coward, M. P. and Dietrich, D.: Alpine tectonics; an overview, in Coward, M. P., Dietrich, D., and Park, R. G. (eds): Alpine Tectonics: Geological Society Special Publications, 45, 1-29, 1989.

Cuffaro, M., Riguzzi, F., Scrocca, D., Antonioli, F., Carminati, E., Livani, M., and Doglioni, C.: On the geodynamics of the northern Adriatic plate. Rend. Fis. Acc. Lincei, 21(1), S253–S279. doi: 10.1007/s12210-010-0098-9, 2010.

D'Ambrogi, C., Maesano, F.E., Marino, M., Congi, M.P., and Morrone, S.: Geological 3D model of the Po Basin. https://doi.org/10.15161/oar.it/76873, 2023.

Dacome, M.C., Miandro, R., Vettorel, M., and Roncari, G.: Subsidence monitoring network: An Italian example aimed at a sustainable hydrocarbon E&P activity. In Proceedings of the International Association of Hydrological Sciences (IAHS), Nagoya, Japan, 15–19 November 2015; Copernicus GmbH: Göttingen, Germany, 372, 379–384, 2015.

Dercourt, J., Zonenshain, L. P., Ricou, L. E., Kazmin, V. G., Le Pichon, X., Knipper, A. L., ... and Pechersky, D. H.: Geological evolution of the Tethys belt from the Atlantic to the Pamirs since the Lias, Tectonophysics, 123(1-4), 241-315, 1986.

Devoti, R., Riguzzi, F., Cuffaro, M., and Doglioni, C.: New GPS constraints on the kinematics of the Apennine subduction, Earth Planet Sci. Lett., 273(1–2), 163–174, https://doi.org/10.1016/j.epsl.2008.06.031, 2008.

Doglioni, C.: A proposal for the kinematic modelling of W-dipping subductions – possible applications to the Tyrrhenian-Apennines system, Terra Nova, 3, 423-434, 1991.

Doglioni, C.: Some remarks on the origin of foredeeps, Tectonophysics, 288, 1-20, 1993.

Domeneghetti, A., Carisi, F., Castellarin, A., and Brath, A.: Evolution of flood risk over large areas: Quantitative assessment for the Po river, J. Hydrol., 527, 809-823, 2015.

European Commission: Urban Europe - Statistics on cities, towns and suburbs, in: M. Kotzeva (ed): General and Regional Statistics (Luxemburg: Collection: Statistical books), available at https://ec.europa.eu/eurostat/web/products-statistical-books/-/ks-01-16-691 (last access: 08/07/2022), 2016.

Faccenna, C., Jolivet, L., Piromallo, C., Morelli, A.: Subduction and the depth of convection in the Mediterranean mantle. J. geophys. Res., 108(B2), 2099, https://doi.org/10.1029/2001JB001690, 2003.

Fantoni, R. and Scotti, P.: Thermal record of the Mesozoic extensional tectonics in the Southern Alps, Atti Ticinesi di Scienza della Terra, 9, 96–101, 2003.

Fantoni, R., Bersezio, R., and Forcella, F.: Alpine structure and deformation chronology at the Southern Alps-Po Plain border in Lombardy. Bollettino della Società geologica italiana, 123(3), 463-476, 2004.Fantoni, R. and Franciosi, R.: Mesozoic extension and Cenozoic compression in Po Plain and Adriatic foreland, Rend. online Soc. Geol. It., 9, 28-31, 2009.

Fantoni, R. and Franciosi R.: Tectono-sedimentary setting of the Po Plain and Adriatic foreland, Rend. Fis. Acc. Lincei, 21 (1), 197-209, doi:10.1007/s12210-010-0102-4, 2010.

Garzanti, E., Vezzoli, G., and Andò, S.: Paleogeographic and paleodrainage changes during Pleistocene glaciations (Po Plain, northern Italy). Earth-Science Reviews, 105(1-2), 25-48, 2011.

Ghielmi, M., Minervini, M., Nini, C., Rogledi, S., Rossi, M., and Vignolo, A.: Sedimentary and tectonic evolution in the eastern Po-Plain and northern Adriatic Sea area from Messinian to Middle Pleistocene (Italy), Rend. Fis. Acc. Lincei, 21(Suppl 1), S131–S166, doi:10.1007/s12210-010-0101-5, 2010.

Ghielmi, M., Minervini, M., Nini, C., Rogledi, S., and Rossi, M.: Late Miocene–Middle Pleistocene sequences in the Po Plain–Northern Adriatic Sea (Italy): the stratigraphic record of modification phases affecting a complex foreland basin, Mar. Pet. Geol. , 42(C), 50-81, https://doi.org/10.1016/j.marpetgeo.2012.11.007, 2013.

Gibbard, P. L., Head, M. J., Walker, M. J. C., and Subcommission on Quaternary Stratigraphy: Formal ratification of the Quaternary System/Period and the Pleistocene Series/Epoch with a base at 2.58 Ma, J. Quaternary Sci., 25, 96–102, https://doi.org/10.1002/jqs.1338, 2010.

Grandić, S., Biancone, M., and Samarz̆ija, J.: Geophysical and stratigraphic evidence of the Adriatic Triassic rift structures, Mem. Soc. Geol. It., 57, 315–325, 2002.

Helliwell, J. F. and Putnam R. D.: Economic Growth and Social Capital in Italy, Eastern Economic Journal, 21, 295-307, 1995.

Hemami, B., Masouleh, S. F., and Ghassemi, A.: 3D geomechanical modeling of the response of the Wilzetta Fault to saltwater disposal, Earth Planet. Phys., 5(6), 559–580, http://doi.org/10.26464/epp2021054, 2021.

Herrera-Garcia, G., Ezquerro, P., Tomás, R., Béjar-Pizarro, M., López-Vinielles, J., Rossi, M., Mateos, R. M., Carreón-Freyre, D., Lambert, J., Teatini, P., Cabral-Cano, E., Erkens, G., Galloway, D., Hung, W. C., Kakar, N., Sneed, M., Tosi, L., Wang, H., Ye, S.: Mapping the global threat of land subsidence, Science, 371 (6524), 34-36, doi:10.1126/science.abb8549, 2021.

International Commission on Hydrocarbon Exploration and Seismicity in the Emilia region: Report on the hydrocarbon exploration and seismicity in Emilia region (213 pp.), International Commission on Hydrocarbon Exploration and Seismicity

in the Emilia region, retrieved from http://mappegis.regione.emilia-romagna.it/gstatico/documenti/ICHESE/ICHESE_Report.pdf (last access: 08/07/2022), 2014.

ISIDe Working Group: Italian Seismological Instrumental and parametric database: http://iside.rm.ingv.it, INGV, 2010.

ISPRA: Modello geologico 3D e geopotenziali della Pianura Padana centrale (Progetto GeoMol), Rapporti ISPRA, 234/2015, pp. 104 e Appendice, 2015

Kint, L., Hademenos, V., De Mol, R., Stafleu, J., Van Heteren, S., and Van Lancker, V.: Uncertainty assessment applied to marine subsurface datasets, Q. J. Eng. Geol. Hydrogeol., 54(1), https://doi.org/10.1144/qjegh2020-028, 2020.

Lindquist, S.J.: Petroleum systems of the Po basin province of Northern Italy and the Northern Adriatic Sea: Porto Garibaldi (Biogenic), Neride/Riva di Solto (Thermal) and Marnoso Arenacea (Thermal), U. S. Department of the Interior, USGS, 1999.

Livani, M., Scrocca, D., Arecco, P., and Doglioni, C.: Structural and stratigraphic control on salient and recess development along a thrust belt front: The Northern Apennines (Po Plain, Italy), J. geophys. Res., Solid Earth, 123, 4360–4387, https://doi.org/10.1002/2017JB015235, 2018.

Livani, M., Scrocca, D., Gaudiosi, I., Mancini, M., Cavinato, G. P., de Franco, R., Caielli, G., Vignaroli, G., Romi, A., and Moscatelli, M.: A geology-based 3D velocity model of the Amatrice Basin (Central Italy), Eng. Geol., 306, 106741, https://doi.org/10.1016/j.enggeo.2022.106741, 2022.

Livani, M., Petracchini, L, Benetatos, C., Marzano, F., Billi, A., Carminati, E., Doglioni, C., Petricca, P., Maffucci, R., Codegone, G., Rocca, V., Verga, F., and Antoncecchi, I.: Digitized geological and geophysical data from the Po Plain and the northern Adriatic Sea (north Italy) collected from public sources. (Version 1.1) [Data set], Zenodo, https://doi.org/10.5281/zenodo.8126519, 2023.

Livio, F. A., Berlusconi, A., Michetti, A. M., Sileo, G., Zerboni, A., Trombino, L., Cremaschi, M., Mueller, K., Vittori, E., Carcano, C., Rogledi, S.: Active fault-related folding in the epicentral area of the December 25, 1222 (Io= IX MCS) Brescia earthquake (Northern Italy): seismotectonic implications. Tectonophysics, 476(1-2), 320-335, https://doi.org/10.1016/j.tecto.2009.03.019, 2009.

Maesano, F. E., D'Ambrogi, C., Burrato, P. and Toscani, G.: Slip-rates of blind thrusts in slow deforming areas: Examples from the Po Plain (Italy), Tectonophysics, 643, 8–25, https://doi.org/10.1016/j.tecto.2014.12.007, 2015.

Maesano, F. E. and D'Ambrogi, C.: Coupling sedimentation and tectonic control: Pleistocene evolution of the central Po Basin. Ital. J. Geosci., 135(3), 394-407, https://doi.org/10.3301/IJG.2015.17, 2016.

Magistrale, H., McLaughlin, K., and Day, S.: A geology-based 3D velocity model of the Los Angeles basin sediments, Bull. Seismol. Soc. Am., 86 (4), 1161–1166, https://doi.org/10.1785/BSSA0860041161, 1996.

Magistrale, H., and Day, S.: 3D simulations of multi-segment thrust fault rupture. Geophysical Research Letters, 26(14), 2093-2096, https://doi.org/10.1029/1999GL900401, 1999.

Malinverno, A. and Ryan, W. B. F.: Extension in the Tyrrhenian Sea and shortening in the Apennines as a result of arc migration driven by sinking of the lithosphere, Tectonics, 5, 227–245. https://doi.org/10.1029/TC005i002p00227, 1986.

Masetti, D., Fantoni, R., Romano, R., Sartorio, D., and Trevisani, E.: Tectonostratigraphic evolution of the Jurassic extensional basins of the eastern southern Alps and Adriatic foreland based on an integrated study of surface and subsurface data, AAPG Bulletin, 96(11), 2065–2089. https://doi.org/10.1306/03091211087, 2012.

845 Molinari, I., Argnani, A., Morelli, A., and Basini, P.: Development and testing of a 3D seismic velocity model of the Po Plain sedimentary basin, Italy, Bull. Seismol. Soc. Am., 105(2A), 753–764, doi:10.1785/0120140204, 2015.

Montone, P., Mariucci, M. T., Pondrelli, S., and Amato, A.: An improved stress map for Italy and surrounding regions (central Mediterranean), J. geophys. Res., 109, B10410, doi:10.1029/2003JB002703, 2004.

Montone, P., Mariucci, M. T., and Pierdominici, S.: The Italian present-day stress map, Geophys. J. Int., 189, 705–716,
850 doi:10.1111/j.1365-246X.2012.05391.x, 2012.

Muttoni, G., Carcano, C., Garzanti, E., Ghielmi, M., Piccin, A., Pini, R., Rogledi, S., and Sciunnach, D.: Onset of major Pleistocene glaciations in the Alps. Geology, 31(11), 989-992, https://doi.org/10.1130/G19445.1 , (2003).

Nicolich, R., Della Vedova, B., Giustiniani, M., and Fantoni, R.: Carta del sottosuolo della Pianura Friulana, 2004.

Ori, G.G.: Continental depositional systems of the Quaternary of the Po Plain (northern Italy). Sediment. Geol. 83, 1–14, 1993.

855 Patacca, E., Sartori, R., and Scandone, P.: Tyrrhenian basin and Apenninic arcs: Kinematic relations since Late Tortonian times, Mem. Soc. Geol. It., 45, 425–451, 1990.

Pezzo, G., Petracchini, L., Devoti, R., Maffucci, R., Anderlini, L., Antoncecchi, I., Billi, A., Carminati, E., Ciccone, F., Cuffaro, M., Livani, M., Palano, M., Petricca, P., Pietrantonio, G., Riguzzi, F., Rossi, G., Sparacino, F. and Doglioni, C.: Active fold-thrust belt to foreland transition in northern Adria, Italy, tracked by seismic reflection profiles and GPS offshore
860 data, Tectonics, 39, e2020TC006425. https://doi.org/10.1029/2020TC006425, 2020.

Picotti, V., Capozzi, R., Bertozzi, G., Mosca, F., Sitta, A., and Tornaghi, M.: The Miocene petroleum system of the Northern Apennines in the central Po Plain (Italy), in: Lacombe, O., Lavé, J., Roure, F., and Vergés, J. (eds), Thrust belts and foreland basins. From fold Kinematics to Hydrocarbon Systems, Springer, 117-131, 2007.

Pieri, M. and Groppi, G.: Subsurface geological structure of the Po Plain, Italy, Progetto finalizzato Geodinamica-
865 Sottoprogetto 5- Modello strutturale, C.N.R., Pubbl. 414, Roma, 1981.

Pieri M.: Three seismic profiles through the Po Plain, in: Bally, A. W. (ed): Seismic Expression of Structural Stiles, AAPG, Studies in Geology. 15 (3.4.1), 8-26, 1983.

Pola, M., Ricciato, A., Fantoni, R., Fabbri, P., and Zampieri, D.: Architecture of the western margin of the North Adriatic foreland: The Schio-Vicenza fault system, Italian Journal of Geosciences, 133(2), 223–234, 2014.

870 Radwan, A., and Sen, S.: Stress Path Analysis for Characterization of In Situ Stress State and Effect of Reservoir Depletion on Present-Day Stress Magnitudes: Reservoir Geomechanical Modeling in the Gulf of Suez Rift Basin, Egypt, Nat. Resour. Res. 30, 463–478, https://doi.org/10.1007/s11053-020-09731-2, 2021.

Ravaglia, A., Seno, S., Toscani, G., and Fantoni, R.: Mesozoic extension controlling the Southern Alps thrust front geometry under the Po Plain, Italy: insights from sandbox models, in: Butler, R.W.H., Tavarnelli, E. and Grasso, M. (eds), Tectonic

875   Inversion and Structural Inheritance in Mountain Belts, Journal of Structural Geology, Special Publication 28, 2084-2096, https://doi.org/10.1016/j.jsg.2006.07.011, 2006.

Regione Emilia-Romagna and ENI-AGIP: Riserve Idriche Sotterranee della Regione Emilia-Romagna: A cura di G. Di Dio, S.EL.CA. s.r.l. (Firenze), 120 p., 1998.

Regione Lombardia and ENI-AGIP: Geologia degli Acquiferi Padani della Regione Lombardia. A cura di C. Carcano & A.
880   Piccin, S.EL.CA. (Firenze), 2002.

Ricci Lucchi, F.: The foreland basin system of the northern Apennines and related clastic wedges: A preliminary outline, Giornale di Geologia, 48(1–2), 165–186, 1986.Rohatgi, A.: WebPlotDigitizer user manual version 3.4. URL http://arohatgi. info/WebPlotDigitizer/app, 1-18, 2014.

Rio, D., Sprovieri, R., Castradori, D., and Di Stefano, E.: The Gelasian Stage (Upper Pliocene): a new unit of the global
885   standard chronostratigraphic scale, Episodes, 21, 82–87, https://doi.org/10.18814/epiiugs/1998/v21i2/002, 1998.

Royden, L.: Flexural behaviour of the continental lithosphere in Italy: constraints imposed by gravity and deflection data, J. Geophys. Res., 93, 7747-7766, https://doi.org/10.1029/JB093iB07p07747, 1988.

Rosenbaum, G. and Lister, G. S.: Neogene and Quaternary rollback evolution of the Tyrrhenian Sea, the Apennines and the Sicilian Maghrebides, Tectonics, 23, TC1013, https://doi.org/10.1029/2003TC001518, 2004.

890   Rovida, A., Locati, M., Camassi, R., Lolli, B., and Gasperini, P.: The Italian earthquake catalogue CPTI15, Bull. Earthq. Eng., 18(7), 2953-2984, https://doi.org/10.1007/s10518-020-00818-y, 2020.

Rovida, A., Locati, M., Camassi, R., Lolli, B., Gasperini, P., and Antonucci, A.: Italian Parametric Earthquake Catalogue (CPTI15), versione 4.0, INGV, https://doi.org/10.13127/CPTI/CPTI15.4, 2022.

Roy, M., and Clayton, R.: Crust and mantle structure beneath the Los Angeles basin and vicinity: constraints from gravity and
895   seismic velocities. EOS Trans. AGU, 80, F251, 1999.

Sangnimnuan, A., Li JW, and Wu, K.: Development of coupled two phase flow and geomechanics model to predict stress evolution in unconventional reservoirs with complex fracture geometry. J. Petrol. Sci. Eng. 196:108072, https://doi.org/10.1016/j.petrol.2020.108072, 2021.

Scardia, G., De Franco, R., Muttoni, G., Rogledi, S., Caielli, G., Carcano, C., Sciunnach, D., and Piccin, A.: Stratigraphic
900   evidence of a Middle Pleistocene climate-driven flexural uplift in the Alps. Tectonics, 31(6), https://doi.org/10.1016/j.quascirev.2012.08.016, 2012.Schutjens, P.M.T.M., Snippe, J.R., Mahani, H., Turner, J., Ita, J., and Mossop, A.P.: Production-induced stress change in and above a reservoir pierced by two salt domes: A geomechanical model and its implications. 72nd SPE EUROPEC/EAGE conference and exhibition, Barcelona, Spain, Extended abstracts L013. SPE J. 17 (01): 80–97, https://doi.org/10.2118/131590-PA, 2010.

905   Scrocca, D., Carminati, E., Doglioni, C., and Marcantoni, D.: Arretramento dello slab adriatico e tettonica compressiva attiva nell'Appennino centro-settentrionale, Rend. Soc. Geol. It., 2, 180-181, 2006.

Scrocca, D., Carminati, E., Doglioni, C., and Marcantoni, D.: Slab retreat and active shortening along the central-northern Apennines, in Lacombe, O., Lav, J., Roure, F., and Vergs, J. (eds): Thrust Belts and Foreland Basins: From Fold Kinematics

to Hydrocarbon Systems, Frontiers in Earth Sciences, Springer, 471–487, https://doi.org/10.1007/978-3-540-69426-7_25,
2007.

Shepard, D.: A two-dimensional interpolation function for irregularly-spaced data. In Proceedings of the 1968 23rd ACM national conference, 517-524, https://doi.org/10.1145/800186.810616, 1968.

Süss, M.P., Shaw, J. H., Komatitsch, D., and Tromp, J.: 3D Velocity and Density Model of the Los Angeles Basin and Spectral Element Method Earthquake Simulations. American Geophysical Union, Fall Meeting 2001, abstract id. S11A-0549, 2001.

Tabellini, G.: Culture and Institutions: Economic Development in the Regions of Europe, J. Eur. Econ. Assoc., 8(4), 677-716, https://doi.org/10.1111/j.1542-4774.2010.tb00537.x, 2010.

Tarquini, S., Isola, I., Favalli, M., and Battistini, A.: TINITALY, a digital elevation model of Italy with a 10 meters cell size (Version 1.0), INGV, https://doi.org/10.13127/TINITALY/1.0, 2007.

Teatini, P., Ferronato, M., and Gambolati, G.: Groundwater pumping and land subsidence in the Emilia-Romagna coastland, Italy: Modeling the past occurrence and the future trend. Water resources research, 42, W01406, doi:10.1029/2005WR004242, 2006.

Tobler, W.: A computer movie simulating urban growth in the Detroit region, Economic Geography, 46(Supplement), 234–240, 1970.

Toscani, G., Burrato, P., Di Bucci, D., Seno, S., and Valensise G.: Plio-Quaternary tectonic evolution of the Northern Apennines thrust fronts (Bologna-Ferrara section, Italy): seismotectonic implications. Ital. J. Geosci. (Boll. Soc. Geol. It.), 128, 2, 605-613, 2009.

Toscani, G., Bonini, L., Ahmad, M. I., Di Bucci, D., Di Giulio, A., Seno, S., and Galuppo, C.: Opposite verging chains sharing the same foreland: Kinematics and interactions through analogue models (Central Po Plain, Italy). Tectonophysics, 633, 268-282, https://doi.org/10.1016/j.tecto.2014.07.019 , (2014).

Turrini, C., Lacombe, O., and Roure, F.: Present-day 3D structural model of the Po Valley basin, Northern Italy, Mar. Pet. Geol., 56, 266-289, https://doi.org/10.1016/j.marpetgeo.2014.02.006, 2014.

Turrini, C., Angeloni, P., Lacombe, O., Ponton, M., and Roure, F.: Three-dimensional seismo-tectonics in the Po Valley basin, Northern Italy, Tectonophysics, 661, 156–79, https://doi.org/10.1016/j.tecto.2015.08.033, 2015.

Wilson, L. F., Pazzaglia, F. J., and Anastasio, D. J.: A fluvial record of active fault-propagation folding, Salsomaggiore anticline, northern Apennines, Italy, J. geophys. Res., 114(B8), https://doi.org/10.1029/2008JB005984, 2009.

Zappaterra, E.: Carbonate paleogeographic sequences of the Periadriatic region, Boll. Soc. Geol. It., 109, 5–20, 1990.

Zerbini, S., Richter, B., Rocca, F., Van Dam, T., and Matonti, F.: A combination of space and terrestrial geodetic techniques to monitor land subsidence: case study, the Southeastern Po Plain, Italy, J. geophys. Res., Solid Earth, 112(B5), https://doi.org/10.1029/2006JB004338, 2007.

Zuffetti, C., and Bersezio, R: Morphostructural evidence of late quaternary tectonics at the Po Plain-Northern Apennines border (Lombardy, Italy). Geomorphology, 364, 107245, https://doi.org/10.1016/j.geomorph.2020.107245, 2020.